haematologica
Journal of the Ferrata Storti Foundation

Bedaquiline amplifies proteasome inhibitor efficacy and overcomes resistance in multiple myeloma

by Michela Cumerlato, Monica Maccagno, Maria Labrador, Beatrice Luciano, Elisabetta Mereu, Mariangela Porro, Cecilia Bandini, Mattia Furlan, Domenico Maisano, Mattia D'Agostino, Alessandra Larocca, Francesca Gay, Annalaura Tamburrini, Francesca Anselmi, Paolo Ettore Porporato, Salvatore Oliviero, Benedetto Bruno, Eugenio Morelli, Nikhil Munshi and Roberto Piva

Received: November 5, 2025.
Accepted: April 16, 2026.

Citation: Michela Cumerlato, Monica Maccagno, Maria Labrador, Beatrice Luciano, Elisabetta Mereu, Mariangela Porro, Cecilia Bandini, Mattia Furlan, Domenico Maisano, Mattia D'Agostino, Alessandra Larocca, Francesca Gay, Annalaura Tamburrini, Francesca Anselmi, Paolo Ettore Porporato, Salvatore Oliviero, Benedetto Bruno, Eugenio Morelli, Nikhil Munshi and Roberto Piva. Bedaquiline amplifies proteasome inhibitor efficacy and overcomes resistance in multiple myeloma.
Haematologica. 2026 Apr 23. doi: 10.3324/haematol.2025.300157 [Epub ahead of print]

Bedaquiline amplifies proteasome inhibitor efficacy and overcomes resistance in multiple myeloma

Michela Cumerlato[1,2], Monica Maccagno[1,2], María Labrador[1,2], Beatrice Luciano[1,2], Elisabetta Mereu[1,2], Mariangela Porro[1,2], Cecilia Bandini[1,2], Mattia Furlan[3], Domenico Maisano[4], Mattia D'Agostino[1,5], Alessandra Larocca[1,5], Francesca Gay[1,5], Annalaura Tamburrini[2,6], Francesca Anselmi[2,6], Paolo Ettore Porporato[1,2], Salvatore Oliviero[2,6], Benedetto Bruno[1,5], Eugenio Morelli[3,7], Nikhil Munshi[4], Roberto Piva[1,2,5]

[1]Department of Molecular Biotechnology and Health Sciences, University of Turin, Turin, Italy;
[2]Molecular Biotechnology Center (MBC) "Guido Tarone", Turin, Italy;
[3]Candiolo Cancer Institute, FPO-IRCCS, Turin, Italy;
[4]Dana Farber Cancer Institute, Boston, MA, United States;
[5]Città della Salute e della Scienza Hospital, Turin, Italy;
[6]Department of Life Sciences and Systems Biology, University of Turin, Turin, Italy;
[7]Department of Oncology, University of Turin, Turin, Italy.

Correspondence: Roberto Piva; e-mail: roberto.piva@unito.it

Running Title: Bedaquiline potentiates PI activity in MM

Keywords: multiple myeloma, proteasome inhibitors, ATP synthase, ATP5F1C, bedaquiline, mitochondrial stress, proteotoxic stress

Data sharing statement: RNA-sequencing and proteomics datasets generated during this study are available from the corresponding author upon reasonable request. Processed data supporting the findings of this study are included in the article and its Supplementary material.

Disclosure/Conflicts of Interest: The authors declare no competing financial interests.

Contributions: M.C., carried out most of the experiments and contributed to the interpretation of biological data together with E.M., M.L., M.P., and M.M.; E.M. performed drug screening experiments and analysis; B.L. studied BDQ combinations with proteasome inhibitors; A.T., M.F., and F.A. performed RNA-Seq experiments and bioinformatics analyses; S.O. supervised bioinformatics analyses; P.E.P. supervised biochemical assays; A.L., M.D.A., F.G. and B.B. provided clinically annotated MM samples; M.C., M.M., and C.B. performed zebrafish xenograft experiments; E.Mo. and N.M. participated in the experimental design and the interpretation of biological data;

R.P. designed the studies and supervised the project; M.C. and R.P. wrote the manuscript; all authors reviewed and approved the final version of the manuscript.

Funding: This work was supported by AIRC (Investigator Grant 21585 to R.P.; Start-Up Grant 29106 to E.Mo.), the University of Torino (RILO 2022–2025 to R.P.), Fondazione CRT (Progetto Ordinario 2022-AI1391 to R.P.), The Leukemia & Lymphoma Society (Special Fellow Grant to E.Mo.), the American Society of Hematology (Scholar Award to E.Mo.), and the Italian Ministry of Health (FPRC “5xmille” 2021 EMAGEN-FaBer and Ricerca Corrente 2024 to E.Mo.).

Acknowledgements: The authors gratefully acknowledge the Advanced Microscopy Open Lab (OLMA@MBC) and Dr. Marta Gai for assistance with image acquisition of zebrafish xenotransplanted embryos; Dr. Lorenzo Prever, and Profs. Giorgio R. Merlo and Emilio Hirsch for their guidance with zebrafish xenograft experiments; Drs. Karel Harant and Pavel Talacko (Laboratory of Mass Spectrometry, BIOCEV, Vestec, Czech Republic) for performing and analyzing the label-free quantitative proteomic experiments; and Drs. Ivan Zaggia, Marcello Turi, and Anna Maria Gullà for their technical and scientific support with metabolic and immunological assays.

ABSTRACT

Proteasome inhibitors (PIs) are cornerstone therapies for multiple myeloma (MM), yet resistance remains a major barrier to durable responses. To identify druggable vulnerabilities that enhance PI efficacy, we performed a small-molecule chemical screen in the presence of carfilzomib (CFZ). We identified bedaquiline (BDQ), an FDA-approved antimycobacterial agent, as a potent synergistic partner. BDQ and its fumarate salt (BDQ-F) significantly amplified CFZ-induced cytotoxicity in PI-sensitive and PI-resistant MM cells, in AL amyloidosis and other B-cell malignancies, with minimal toxicity toward normal cells. Mechanistic studies confirmed that BDQ specifically targets the ATP5F1C subunit of mitochondrial ATP synthase. BDQ-CFZ combination triggered extensive apoptosis, exacerbating proteotoxic stress and proteasome-associated pathways. BDQ specifically enhanced CFZ's inhibition of the proteasome's chymotrypsin-like activity. Importantly, BDQ synergized with multiple proteasome and ubiquitin-activating enzyme inhibitors, but not with other standard MM agents, underscoring its selective interaction with the UPS pathway. BDQ-CFZ co-treatment markedly reduced MM cell viability and tumor burden in patient-derived cells and zebrafish xenograft models. These findings support the therapeutic repurposing of BDQ to potentiate PI efficacy and overcome resistance in MM and related B-cell malignancies.

INTRODUCTION

Multiple myeloma (MM) is a malignancy of terminally differentiated B cells marked by clonal plasma cell expansion in the bone marrow and excess monoclonal immunoglobulin production (1). It is the second most common hematologic cancer in high-income countries, typically diagnosed between ages 60 and 70 (2). Standard frontline therapies combine proteasome inhibitors (PIs), immunomodulatory agents, corticosteroids, and monoclonal antibodies targeting CD38 (3-5). Recently, CAR T cells and bispecific T cell engagers (BiTEs) have shown remarkable efficacy in heavily pretreated relapsed/refractory MM patients (6, 7). While these regimens have improved survival, MM remains incurable due to intrinsic and acquired resistance mechanisms (8, 9). Identifying new vulnerabilities and combinatorial strategies to enhance efficacy while reducing toxicity is essential (10). However, MM's extensive genetic and epigenetic heterogeneity complicates treatment and fuels resistance (11, 12). To address this, omics-driven approaches and ex vivo functional screens are increasingly used to identify actionable targets (13). MM cells exhibit high proteostasis stress due to their immunoglobulin load, making them susceptible to Pis (14). Yet, metabolic and epigenetic reprogramming enable adaptation and drug resistance (15, 16). Targeting these compensatory pathways offers a rational strategy to resensitize cells to PIs. We previously identified several PI synergistic interactors, including IDH2 and LSD1, as actionable nodes to restore PI sensitivity (17-19). Here, we describe the FDA-approved ATP synthase inhibitor bedaquiline (BDQ) (20) as a novel synergistic partner of the PI carfilzomib (CFZ). BDQ-CFZ co-treatment selectively induces proteotoxic stress and apoptosis in MM cells. Given BDQ's established safety and clinical availability, our findings support its repurposing to enhance PIs efficacy and overcome resistance in MM and potentially other B-cell malignancies.

METHODS

Detailed experimental procedures for cell culture conditions, reagents, cellular and biochemical assays, plasmids, virus production, RNA extraction, reverse transcription-quantitative PCR, western blotting, RNA sequencing, proteomics, and data analyses are included in Supplemental Material and Methods.

Drug screening

Primary compound screening was performed using a selective small-molecule inhibitor library (L3500, Selleck Chemicals) consisting of 320 inhibitors targeting 123 key proteins involved in diverse signaling pathways. U-266^{PIR} multiple myeloma (MM) cells were treated with each compound at four concentrations (10 μM, 1 μM, 100 nM, and 10 nM). After 2 hours, cells were exposed to either a sublethal dose of carfilzomib (CFZ; 20 nM) or dimethyl sulfoxide (DMSO) as a vehicle control. Cell viability was measured at baseline (0 h) and 72 hours post-treatment using the CellTiter-Glo Luminescent Cell Viability Assay (Promega), and results were collected in duplicate. Growth rate (GR) was calculated by normalizing the luminescent signal at 72 hours to the baseline signal and further normalized to the DMSO-treated controls. Drug combination effects were quantified using the Excess Over Bliss (EOB) model, calculated from GR values using the following formula: [1 − GR(combination)] – [1 − GR(CFZ)] – [1−GR(drug)] + [1−GR(CFZ)][1 − GR(drug)] (21). Compounds yielding EOB ≥ 0.4 at any concentration were considered potential hits and shortlisted for secondary validation in a panel of five MM cell lines (U-266PIR, U-266, KMM-1, AMO-1, and KMS-28). Compounds that achieved EOB ≥ 0.4 in at least three cell lines were designated top synergistic candidates (TOP14) and listed in Supplementary Table S1.

MM Patient and Healthy Donor Samples

Peripheral blood mononuclear cells (PBMCs) from healthy donors and bone marrow (BM) aspirates from MM patients were obtained from the local Blood Bank (Città della Salute e della Scienza Hospital, Turin). PBMCs were isolated from buffy coats via Ficoll-Hypaque density gradient, resuspended in RPMI + 10% FBS, and seeded at 5×10^5 cells/mL. BM mononuclear cells were isolated by Ficoll gradient centrifugation following Miltenyi's protocol. $CD138^+$ plasma cells were identified by flow cytometry using anti-CD138-APC (clone 44F9, Miltenyi), and samples with ≥10% $CD138^+$ cells were used for downstream assays. Cells were seeded at 2.5×10^5 cells/mL in RPMI + 10% FBS and treated as described in Supplementary Table S2.

Zebrafish Xenograft Assay

Approximately 250 RPMI-8226 cells stably expressing DsRed fluorescent protein were injected (2 nL) into the yolk sac of 48 hours post-fertilization (hpf) embryos with a manual microinjector (Eppendorf, Germany). Embryos were maintained at 28°C in embryo medium supplemented with 0.003% PTU, 1 g/L glucose, and 5 mM L-glutamine. At 24 hours post-injection (hpi), xenograft-positive embryos were identified by fluorescence microscopy (ZEISS Axio Observer, 10× objective), randomly allocated into four treatment groups (DMSO, 2.5 nM CFZ, 10 µM BDQ, or combination), and placed individually into 48-well plates. Tumor burden was assessed at 72 hpi by fluorescence microscopy and quantified using ImageJ as the fluorescence area normalized to the 24 hpi baseline. Adult zebrafish were euthanized with a tricaine overdose. All procedures were approved by the Local Ethical Committee and the Italian Ministry of Health.

Ethics Approval And Consent To Participate

PBMCs from healthy donors and bone marrow aspirates from MM patients were obtained from the local Blood Bank and the Hematology Unit at Città della Salute e

della Scienza Hospital (Turin, Italy). Informed consent was obtained from all participants following the Declaration of Helsinki, and the study was approved by the local ethics committee (protocol no. 00143/2022). All animal experiments were conducted in compliance with institutional guidelines and approved by the Ethical Committee of the University of Torino.

RESULTS

Bedaquiline Synergistically Enhances Proteasome Inhibitor Efficacy in Multiple Myeloma and Other Hematological Malignancies Through ATP5F1C Modulation

To identify compounds that enhance carfilzomib (CFZ) efficacy in multiple myeloma (MM), we performed a functional screen of 320 small-molecule inhibitors in the MM PI-resistant cells U-266^{PIR}, in the presence or absence of sublethal CFZ dose (Fig. 1A). Top candidates were validated in five MM cell lines. Bedaquiline (BDQ) and its fumarate form (BDQ-F), approved to treat multidrug-resistant tuberculosis, showed strong synergy with CFZ in 5 and 3 out of 5 lines, respectively (Supplementary Table S1), and were prioritized for further study. BDQ and BDQ-F strongly synergized with CFZ in almost all tested PI-resistant and PI-sensitive MM cell lines (Fig. 1B–C; Supplementary Fig. 1A–B). The combination also enhanced cytotoxicity in systemic AL amyloidosis, mantle cell lymphoma, diffuse large B-cell lymphoma, and Burkitt's lymphoma (Fig. 1D). Importantly, the BDQ-CFZ combination showed no synergistic toxicity in peripheral blood mononuclear cells (PBMCs) from healthy donors, immortalized B-lymphocytes (IST EBV TW6B), and bone marrow-derived stromal cells (HS-5) (Fig. 2A-C).

To confirm that BDQ-CFZ synergy is mediated via ATP synthase inhibition, we tested the alternative oligomycin-derived ATP synthase inhibitor 1 (ATPSi). ATPSi-CFZ co-

treatment significantly reduced viability of AMO-1 and RPMI-8226 cells, including their PI-resistant derivatives ($p < 0.0001$; Fig. 2D). Accordingly, ATP5F1C knockdown sensitized AMO-1 cells to CFZ ($p < 0.0001$; Fig. 2E; Supplementary Fig. 2A–B), Conversely, ATP5F1C overexpression mitigated BDQ-CFZ-induced cytotoxicity ($p < 0.0001$; Fig. 2F; Supplementary Fig. 2C-D). Collectively, these results demonstrate that BDQ and BDQ-F synergize with CFZ across diverse hematological malignancies, selectively inducing cytotoxicity via modulation of ATP5F1C, without harming healthy cells.

BDQ Potentiates Proteasome Inhibition and Specifically Synergizes with Proteasome Inhibitors in Multiple Myeloma

To elucidate the basis of BDQ-CFZ synergy in MM, we first profiled early apoptotic and stress responses. Immunoblotting of RPMI-8226 and AMO-1 cells 16 hours post-treatment revealed robust activation of caspase-3, PARP cleavage, and increased phosphorylation of H2A.X and RPA32, indicating enhanced apoptosis and DNA damage (Fig. 3A; Supplementary Fig. 3A). BDQ–CFZ co-treatment significantly reduced oxygen consumption rate (OCR) and increased mitochondrial ROS levels compared to single treatments (Supplementary Fig. 2E–F). In MM cells, BDQ exposure alone decreased oxidative phosphorylation; however, ATP5F1C protein abundance was not detectably altered following BDQ treatment (Supplementary Fig. 2G) (22). Transcriptomic profiling of AMO-1 cells 12 hours post-treatment, prior to detectable viability loss (Supplementary Fig. 4A–C), revealed 246 differentially expressed genes in response to CFZ, whereas BDQ alone had minimal transcriptional effects. Strikingly, BDQ-CFZ co-treatment led to 1,492 differentially expressed genes (Fig. 3B). These included upregulation of autophagy, proteasome catabolism, ER

stress, and oxidative phosphorylation pathways, alongside downregulation of cell cycle and migration-related genes (Fig. 3C). Gene set enrichment analysis (GSEA) further demonstrated coordinated activation of stress and proteostasis-related programs, including unfolded protein response, ubiquitin–proteasome–associated processes, and mitochondrial stress pathways such as mitophagy (Supplementary Figs. 5–6). Cell-cycle–related programs were also perturbed, consistent with measurable alterations in cell-cycle distribution observed in MM cells (Supplementary Figs. 3D–E and 4G–H). Notably, BDQ enhanced CFZ-induced expression of proteasome subunits (Fig. 3D), consistent with previously described compensatory feedback mechanisms (23). Independent RT-qPCR analysis confirmed several of the most prominently upregulated and downregulated genes (Fig. 3E; Supplementary Fig. 4D–F). Complementary label-free quantitative proteomics further substantiated the synergistic impact of BDQ-CFZ treatment, revealing a marked increase in upregulated proteins compared to single-agent exposure (Fig. 3F). Integrated analysis of transcriptomic and proteomic data highlighted convergent activation of cellular stress-response pathways (Supplementary Fig. 7).

Importantly, we observed that BDQ potentiated CFZ-mediated chymotrypsin-like proteasome inhibition across MM cell lines, but not in low-responder U-266 cells (Fig. 4A). This enhancement was selective to chymotrypsin-like activity, as caspase-like and trypsin-like activities remained largely unaffected (Supplementary Fig. 8A-B). Proteasome blockade was confirmed in AMO-1 and AMO-1^{BTZR} cells by expressing a short-lived GFP fusion protein (Ub-G76V-GFP), showing increased GFP signal following BDQ-CFZ treatment, before cell death commitment (Fig. 4B-C; Supplementary Fig. 8C-E). BDQ synergized with other PIs, including BTZ, IXA, and MRZ, as well as the ubiquitin-activating enzyme inhibitor TAK-243 across a broad

range of PI-sensitive and PI-resistant MM cell lines (Fig. 4E-H; Supplementary Fig. 9). However, no synergy was observed with standard agents (e.g., dexamethasone, venetoclax, lenalidomide, melphalan, or doxorubicin), underscoring the specificity of BDQ's interaction with ubiquitin-proteasome system (UPS) targeting drugs (Supplementary Fig. 10). Together, these findings reveal that BDQ-CFZ co-treatment induces broad transcriptional and proteomic stress responses, selectively enhancing proteasome inhibition and cytotoxicity in MM cells.

BDQ-CFZ Potentiates Proteasome Inhibition in Patient-Derived and In Vivo Models

To assess the translational potential of BDQ-CFZ, we tested its efficacy in 2D and 3D co-culture systems with HS-5 stromal cells, mimicking the bone marrow niche. The combination significantly increased MM cell death over time in both settings, while sparing stromal cells (Fig. 5A–B; Supplementary Fig. 11), demonstrating selective activity even in protective microenvironments. Public gene expression data highlighted that ATP5F1C is upregulated in NDMM and RRMM vs. healthy donors, and more highly expressed in RRMM than in MGUS (Fig. 5C). Analysis of the CoMMpass IA21 cohort (n = 631) showed that high ATP5F1C expression (top 30% of the distribution) was significantly associated with inferior progression-free survival (PFS) and overall survival (OS) (log-rank adjusted $p = 9.2\times10^{-4}$ and 4.7×10^{-4}, respectively; Fig. 5D–E). In multivariable Cox proportional hazards models adjusting for age and the CGS high-risk classification, as recently defined by the International Myeloma Society and the International Myeloma Working Group (24), ATP5F1C expression retained independent prognostic significance for both PFS and OS (Supplementary Fig. 12A). In contrast, ATP5F1A and ATP5F1B expression did not show comparable

associations with survival outcomes in the same cohort (Supplementary Fig. 12B–E). Ex vivo treatment of $CD138^+$ cells from 13 MM patient bone marrow samples showed that BDQ significantly enhanced CFZ-induced cytotoxicity, regardless of cytogenetic background or treatment history ($p < 0.01$; Fig. 5F; Supplementary Table S2). Finally, in a zebrafish xenograft model, BDQ-CFZ reduced $DsRed^+$ tumor burden (Fig. 5G), confirming in vivo efficacy. These findings support the safety, specificity, and clinical relevance of BDQ-CFZ therapy for MM, and highlight ATP5F1C as a potential biomarker for therapeutic response.

DISCUSSION

The present study demonstrates that the ATP synthase inhibitor BDQ, along with its fumarate salt form (BDQ-F), exhibits consistent and robust synergy with agents targeting the UPS across various MM models, as well as in amyloidosis and diverse B-cell malignancies. BDQ is an orally bioavailable antimicrobial agent originally developed to inhibit ATP synthase in *Mycobacterium tuberculosis*, and has revolutionized the therapeutic landscape for multidrug-resistant tuberculosis (25). In addition, BDQ can inhibit the γ-subunit of human mitochondrial ATP synthase, ATP5F1C (26). Importantly, ATP5F1C plays an essential role in mitochondrial ATP production and has been linked to increased tumor aggressiveness and adverse clinical outcomes (22, 27). Mechanistic validation using both genetic knockdown and pharmacologic inhibition of ATP5F1C phenocopied BDQ-CFZ cytotoxicity, while overexpression conferred resistance, thereby confirming ATP5F1C as the key functional target. Transcriptomic and proteomic analyses revealed that BDQ co-treatment with CFZ amplified stress-response pathways, inducing DNA damage, apoptosis, and proteotoxic stress. Although BDQ–CFZ induced measurable

alterations in cell-cycle distribution, these effects were not uniform across MM models and did not reflect a consistent cytostatic arrest. Instead, they likely represent context-dependent consequences of stress-induced apoptosis. Importantly, BDQ potentiated CFZ-mediated inhibition of chymotrypsin-like proteasome activity. This suggests that BDQ, by impairing ATP production and disrupting oxidative phosphorylation, exacerbates proteotoxic stress induced by proteasome inhibition. While BDQ has been reported to reduce ATP5F1C protein abundance in metastatic breast cancer models (22), we did not detect changes in ATP5F1C protein levels in MM cells despite impaired mitochondrial respiration, suggesting functional modulation of ATP synthase activity rather than altered protein abundance. In addition to these stress-related programs, we observed down-modulation of GPRC5D expression following BDQ–CFZ treatment. Given the ongoing clinical development of GPRC5D-targeting immunotherapies, modulation of antigen expression may be relevant when considering treatment sequencing or combination strategies (28, 29). However, the biological functions and regulatory pathways of GPRC5D in MM remain incompletely defined, and its role in proliferation or drug resistance has not been fully elucidated (29). Further studies will be required to clarify the functional and therapeutic implications of GPRC5D modulation. While HS5 stromal cells enabled reproducible assessment of BDQ–CFZ activity in a bone marrow–mimicking setting, evaluation of this combination in primary bone marrow–derived stromal co-cultures will be important to further delineate its impact within a patient-specific microenvironment.

Beyond the mechanistic evidence, survival analyses in the CoMMpass cohort further supported the clinical significance of ATP5F1C. The independent prognostic impact of ATP5F1C expression, even after adjustment for age and contemporary high-risk cytogenetic classification, underscores the clinical relevance of mitochondrial ATP

synthase activity in multiple myeloma biology. These findings suggest that elevated ATP5F1C expression captures a component of disease aggressiveness not fully explained by established genomic risk features. Notably, the lack of comparable prognostic significance for ATP5F1A and ATP5F1B further supports the specific relevance of the γ subunit in MM progression.

The observed synergy highlights a therapeutic opportunity to exploit metabolic vulnerabilities to overcome PI resistance. By acting through energy stress pathways, BDQ may circumvent canonical resistance mechanisms and sensitize cells to UPS-targeted therapy. Although zebrafish models provide robust in vivo proof-of-concept validation, further evaluation of BDQ–CFZ activity in murine xenograft systems will be important to define its pharmacological and translational potential in mammalian contexts. Importantly, BDQ's clinical approval supports translational development; however, its preferential inhibition of mycobacterial ATP synthase at submicromolar concentrations (24) raises important pharmacological considerations. The effective in vivo dosing required to achieve sustained inhibition of mitochondrial ATP synthase in cancer cells remains to be defined, and more selective inhibitors targeting the γ subunit of mitochondrial ATP synthase should be developed. It also remains to be determined whether inhibition of other subunits (e.g., α or β) would confer comparable antitumor synergy. In addition, ATP depletion may disrupt broader mitochondrial functions or intersect with the tricarboxylic acid cycle, contributing to cytotoxicity. Dissecting these downstream consequences will be essential to fully elucidate the mechanism of action and to rationally design future combination regimens.

In summary, this study supports a therapeutic strategy combining proteasomal and metabolic stress to restore drug sensitivity in MM. The clinical availability of BDQ offers a translational opportunity, while future work should refine target specificity, optimize

pharmacological parameters, and explore this approach in other malignancies characterized by proteotoxic stress.

REFERENCES

1. Kumar SK, Rajkumar V, Kyle RA, et al. Multiple myeloma. Nat Rev Dis Primers. 2017;3(1):17046.
2. van de Donk N, Pawlyn C, Yong KL. Multiple myeloma. Lancet. 2021;397(10272):410-427.
3. Costa LJ, Gay F, Landgren O, et al. Evolution of frontline treatment for multiple myeloma: clinical investigation of quadruplets containing carfilzomib and anti-CD38 monoclonal antibodies. Ann Hematol. 2025;104(3):1329-1351.
4. Kumar SK, Callander NS, Adekola K, et al. NCCN guidelines(R) insights: multiple myeloma, version 1.2025. J Natl Compr Canc Netw. 2025;23(5):132-140.
5. Sonneveld P, Dimopoulos MA, Boccadoro M, et al. Daratumumab, bortezomib, lenalidomide, and dexamethasone for multiple myeloma. N Engl J Med. 2024;390(4):301-313.
6. Jurczyszyn A, Bator M, Vesole DH, et al. New therapies in multiple myeloma: benefits and limitations. Pol Arch Intern Med. 2025;135(4):16994.
7. Neri P, Leblay N, Lee H, et al. Just scratching the surface: novel treatment approaches for multiple myeloma targeting cell membrane proteins. Nat Rev Clin Oncol. 2024;21(8):590-609.
8. Gay F, Marchetti E, Bertuglia G. Multiple myeloma unpacked. Hematol Oncol. 2025;43(Suppl 2):e70067.
9. Mitsiades CS. Proteasome Inhibitors in Multiple myeloma: biological insights on mechanisms of action or resistance informed by functional genomics. Hematol Oncol Clin North Am. 2024;38(2):321-336.
10. Setton J, Zinda M, Riaz N, et al. Synthetic lethality in cancer therapeutics: the next generation. Cancer Discov. 2021;11(7):1626-1635.
11. Manier S, Salem KZ, Park J, et al. Genomic complexity of multiple myeloma and its clinical implications. Nat Rev Clin Oncol. 2017;14(2):100-113.
12. Maura F, Rajanna AR, Ziccheddu B, et al. Genomic classification and individualized prognosis in multiple myeloma. J Clin Oncol. 2024;42(11):1229-1240.
13. Kropivsek K, Kachel P, Goetze S, et al. Ex vivo drug response heterogeneity reveals personalized therapeutic strategies for patients with multiple myeloma. Nat Cancer. 2023;4(5):734-753.
14. Fricker LD. Proteasome inhibitor drugs. Annu Rev Pharmacol Toxicol. 2020;60:457-476.
15. Milan E, Gulla A. Editorial: Proteomic and metabolic reprogramming in myeloma cells within the tumor microenvironment. Front Oncol. 2023;13:1264740.
16. Renatino Canevarolo R, Sudalagunta PR, Meads MB, et al. Epigenetic plasticity drives carcinogenesis and multi-therapy resistance in multiple myeloma. Research Square. 2025 Apr 14. https://doi.org/10.21203/rs.3.rs-6306816/v1 [preprint, not peer-reviewed].
17. Bandini C, Mereu E, Paradzik T, et al. Lysin (K)-specific demethylase 1 inhibition enhances proteasome inhibitor response and overcomes drug resistance in multiple myeloma. Exp Hematol Oncol. 2023;12(1):71.
18. Bergaggio E, Riganti C, Garaffo G, et al. IDH2 inhibition enhances proteasome inhibitor responsiveness in hematological malignancies. Blood. 2019;133(2):156-167.

19. Mereu E, Abbo D, Paradzik T, et al. Euchromatic histone lysine methyltransferase 2 inhibition enhances carfilzomib sensitivity and overcomes drug resistance in multiple myeloma cell lines. Cancers (Basel). 2023;15(8):2199.
20. Zhang Y, Lai Y, Zhou S, et al. Inhibition of M. tuberculosis and human ATP synthase by BDQ and TBAJ-587. Nature. 2024;631(8020):409-414.
21. Niepel M, Hafner M, Duan Q, et al. Common and cell-type specific responses to anti-cancer drugs revealed by high throughput transcript profiling. Nat Commun. 2017;8(1):1186.
22. Fiorillo M, Scatena C, Naccarato AG, Sotgia F, Lisanti MP. Bedaquiline, an FDA-approved drug, inhibits mitochondrial ATP production and metastasis in vivo, by targeting the gamma subunit (ATP5F1C) of the ATP synthase. Cell Death Differ. 2021;28(9):2797-2817.
23. Meiners S, Heyken D, Weller A, et al. Inhibition of proteasome activity induces concerted expression of proteasome genes and de novo formation of Mammalian proteasomes. J Biol Chem. 2003;278(24):21517-21525.
24. Avet-Loiseau H, Davies FE, Samur MK, et al. International Myeloma Society/International Myeloma Working Group Consensus Recommendations on the definition of high-risk multiple myeloma. J Clin Oncol. 2025;43(24):2739-2751.
25. Guglielmetti L, Khan U, Velasquez GE, et al. Oral regimens for rifampin-resistant, fluoroquinolone-susceptible tuberculosis. N Engl J Med. 2025;392(5):468-482.
26. Luo M, Zhou W, Patel H, et al. Bedaquiline inhibits the yeast and human mitochondrial ATP synthases. Commun Biol. 2020;3(1):452.
27. Wu X, Li F, Wang X, et al. Antibiotic bedaquiline effectively targets growth, survival and tumor angiogenesis of lung cancer through suppressing energy metabolism. Biochem Biophys Res Commun. 2018;495(1):267-272.
28. Lee H, Ahn S, Gonzales GA, et al. Multimodal antigenic escape to GPRC5D-targeted T cell engagers in multiple myeloma. Nat Med. 2026;32(3):964-977.
29. Wang X, Cui Y, Wang Y, Fang B. Emerging role of G protein-coupled receptor class C group 5 member D-directed immunotherapy in multiple myeloma: Advances, resistance and combination strategies. Br J Haematol. 2025;207(5):1765-1778.

FIGURE LEGENDS

Figure 1. Bedaquiline synergistically enhances proteasome inhibitor efficacy in multiple myeloma and other hematological malignancies (A) Schematic overview of the functional drug screening strategy used to identify compounds that potentiate carfilzomib (CFZ) activity. A library of 320 small-molecule inhibitors was screened in U-266 PI-resistant (PIR) MM cells, with or without sublethal doses of CFZ. Top hits were validated in a secondary screen across five MM cell lines, identifying bedaquiline (BDQ) and its fumarate salt (BDQ-F) as strong synergistic partners of CFZ. **(B–C)** Cell viability heatmaps showing the synergistic effects of BDQ and CFZ in PI-resistant (B) and PI-sensitive (C) MM cell lines. Data represent the mean of three independent experiments. Compound concentrations, detection methods, time points, and mean ± SD values are provided in Supplementary Tables S3–S4. **(D)** Heatmap summarizing cell viability in systemic light chain amyloidosis (AL) and B-cell non-Hodgkin lymphoma (NHL) cell lines, including germinal center B-cell–like (GCB) and activated B-cell–like (ABC) diffuse large B-cell lymphoma (DLBCL), Burkitt's lymphoma (BL), and mantle cell lymphoma (MCL), following treatment with BDQ, CFZ, or their combination. Viability was measured by PI staining at 96 hours in AL cell lines, and by TMRM staining at 72 hours in B-cell NHL lines. Statistical significance was determined using one-way ANOVA (****$p < 0.0001$).

Figure 2. BDQ-CFZ co-treatment selectively induces cytotoxicity in multiple myeloma cells via ATP5F1C modulation. (A-C) Dose–response matrices showing cell viability after BDQ-CFZ co-treatment in normal human cell models: **(A)** peripheral blood mononuclear cells (PBMCs) from 12 healthy donors; **(B)** EBV-transformed B lymphocytes (IST EBV TW6B; n = 3); **(C)** HS-5 bone marrow stromal cells (n = 3). Viability was measured by PI staining (PBMCs) or TMRM staining (IST EBV TW6B, HS-5) 96 hours post-treatment. **(D)** Viability of PI-sensitive (AMO-1, RPMI-8226) and PI-resistant (AMO-$1^{CFZ\text{-}R}$, AMO-$1^{BTZ\text{-}R}$, RPMI-$8226^{CFZ\text{-}R}$, and RPMI-$8226^{BTZ\text{-}R}$) MM cells treated with ATPSi, CFZ, or their combination. Viability was assessed 72 hours post-treatment using TMRM staining and flow cytometry. **(E)** Viability of AMO-1 cells expressing shCTRL or sh2_ATP5F1C treated with 3 nM CFZ or vehicle (DMSO), measured by TMRM staining 72 hours post-treatment. **(F)** Viability of AMO-1 cells transduced with pLX304 or pLX304_ATP5F1C and treated with 2.5 µM BDQ, 2.5 nM

CFZ, the combination, or vehicle (DMSO). Viability was assessed 6 days post-treatment by TMRM staining and flow cytometry. Data represent the mean ± SD from three independent experiments unless otherwise indicated. Statistical significance was assessed using one-way ANOVA (****$p < 0.0001$).

Figure 3. BDQ-CFZ co-treatment triggers global transcriptional reprogramming and proteotoxic stress in multiple myeloma cells. (A) Immunoblot analysis of apoptotic and DNA damage markers in AMO-1 cells treated for 16 hours with BDQ (5 μM), CFZ (2.5 nM), their combination (BDQ-CFZ), or left untreated (NT). α-Tubulin and β-actin were used as loading controls. **(B)** RNA sequencing analysis of AMO-1 cells reveals extensive transcriptional remodeling following BDQ-CFZ treatment. Bar plot: number of differentially expressed genes (DEGs) relative to untreated controls. Heatmap: hierarchical clustering of DEGs across treatment groups. **(C)** Gene ontology (GO) enrichment analysis of DEGs in BDQ-CFZ-treated cells, identifying upregulation of pathways involved in autophagy, endoplasmic reticulum (ER) stress, hypoxia, proteasomal degradation, ATP metabolism, and oxidative phosphorylation. **(D)** Heatmap of KEGG-defined proteasome gene expression showing transcriptional upregulation of proteasome components in BDQ-CFZ-treated cells. **(E)** Volcano plot of transcriptional changes comparing BDQ-CFZ vs. CFZ treatment. Red: significantly upregulated genes; light blue: significantly downregulated genes; gray: non-significant. **(F)** Volcano plots of label-free quantitative proteomics comparing protein expression changes in AMO-1 cells treated with BDQ, CFZ, or the combination (BDQ-CFZ). Yellow: upregulated; light blue: downregulated.

Figure 4. BDQ potentiates proteasome inhibition and selectively synergizes with proteasome-targeting agents in multiple myeloma. (A) Chymotrypsin-like proteasome activity was measured 5 hours after treatment with BDQ (5 μM or 10 μM for U-266), CFZ (2.5 nM), or their combination in a panel of MM cell lines (AMO-1, KMS-11, RPMI-8226, MOLP-8, and U-266). BDQ significantly enhanced CFZ-mediated proteasome inhibition in all cell lines except U-266, which showed reduced sensitivity to the combination. **(B-C)** Quantification of proteasome inhibition using a Ub-G76V-GFP reporter assay in AMO-1 and AMO-$1^{BTZ\text{-}R}$ cells. Flow cytometry analysis shows increased GFP accumulation upon BDQ-CFZ treatment, indicating enhanced proteasome inhibition. Fluorescence intensity is normalized to untreated

controls and represents the average of three independent experiments (mean ± SD). Statistical analysis confirms significant synergy in both parental and resistant cells (****p < 0.0001, one-way ANOVA). **(D-G)** Heatmap representing cell viability of AMO-1 **(D)** and AMO-1 $^{CFZ-R}$ **(F)** cell lines treated with increasing concentration of carfilzomib (CFZ), bortezomib (BTZ), ixazomib (IXA), marizomib (MAR) and TAK-243 (TAK) in the presence or absence of 10 µM BDQ. The tables indicate the Bliss Score (BS) for AMO-1 **(E)** and AMO-1 $^{CFZ-R}$ **(G)** for each compound tested in the presence of BDQ. Strong synergistic combination scores are highlighted in green, mild synergistic scores in yellow, and non-synergistic ones in red. Cell viability was measured with ATPLite 72 hours post-treatment.

Figure 5. BDQ-CFZ combination enhances MM cell death in patient-derived samples and in vivo models. (A–B) BDQ-CFZ co-treatment potentiates MM cell death in bone marrow–mimicking microenvironments. **(A)** AMO-1 cells were cultured in 2D with GFP+ HS-5 stromal cells and treated with DMSO (NT), BDQ (5 µM), CFZ (2.5 nM), or their combination at day 0 and day 3. Cell viability was assessed by flow cytometry using propidium iodide exclusion, followed by identification of myeloma cells based on CD138 expression. Data are expressed as the percentage of viable MM cells within the total live cell population at the indicated time points (left). Statistical analysis: two-way ANOVA (n = 2–3). **(B)** In a 3D co-culture system, GFP+ HS-5 stromal cells and tRFP+ SK-MM1 MM cells were seeded into scaffolds and treated with CFZ (6 nM), BDQ (10 µM), or their combination. MM cell viability was quantified by flow cytometry 6 days post-treatment by gating on live cells and identifying MM cells based on fluorescent labeling. BDQ-CFZ co-treatment significantly reduced the viability of MM cells compared to single agents (Tukey's multiple comparisons test, p = 0.0242; n = 3–4). *P < 0.05; **P < 0.01; ***P < 0.001. **(C)** ATP5F1C expression increases with disease progression across healthy donors (HD), MGUS, SMM, NDMM, and RRMM groups (data from GSE2658, GSE5900, GSE31161). **(D-E)** High ATP5F1C expression is associated with inferior overall survival (OS) and progression-free survival (PFS) in multiple myeloma patients from the CoMMpass study (IA21, n = 631). Patients were stratified according to ATP5F1C expression (top 30% vs remaining patients). Statistical significance was assessed using the log-rank test with correction for multiple testing. **(F)** BDQ enhances CFZ-induced cytotoxicity in primary MM cells. BMMCs from 13 MM patients were treated with CFZ, BDQ, or the

combination for 96 hours. Viability was assessed by flow cytometry using PI and CD138 stainings and normalized to DMSO controls. Drug concentrations for each patient are listed in Supplementary Table S5. **(G)** In vivo validation using a zebrafish xenograft model. RPMI-8226 cells (tRFP+) were injected into zebrafish embryos and treated with BDQ, CFZ, or their combination. Tumor burden at 72 hours post injection (hpi) was normalized to tumor area at 24 hpi (DMSO: n = 15; CFZ: n = 16; BDQ: n = 13; BDQ-CFZ: n = 14). Abbreviations: PBMCs, peripheral blood mononuclear cells; BMMCs, bone marrow mononuclear cells; s.e.m., standard error of the mean; hpi, hours post-injection; HD, healthy donors; MGUS, monoclonal gammopathy of undetermined significance; SMM, smoldering MM; NDMM, newly diagnosed MM; RRMM, relapsed/refractory MM.

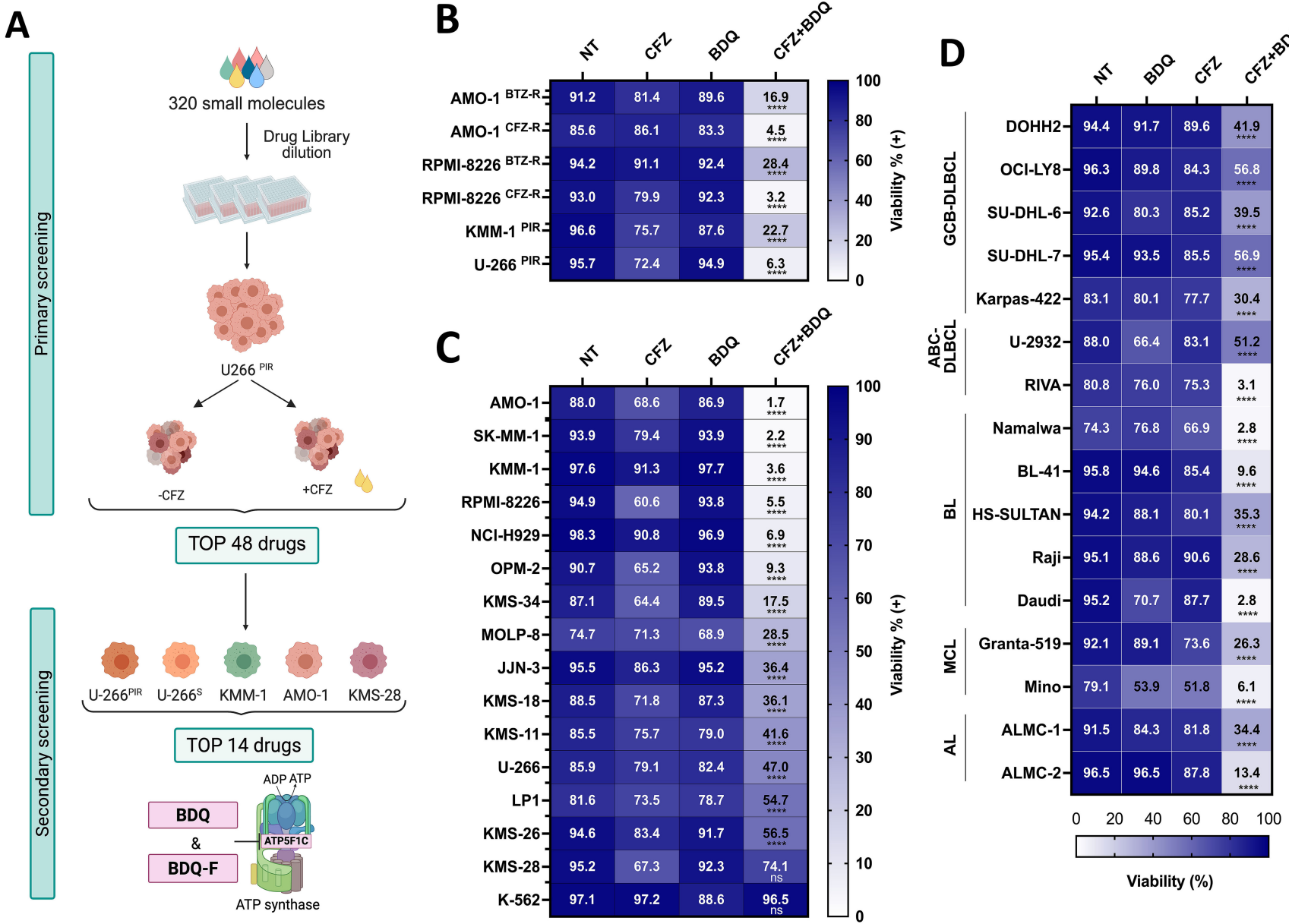
A
Primary screening
320 small molecules
Drug Library dilution
U266 PIR
-CFZ
+CFZ
TOP 48 drugs
Secondary screening
U-266PIR
U-266S
KMM-1
AMO-1
KMS-28
TOP 14 drugs
ADP ATP
BDQ
&
BDQ-F
ATP5F1C
ATP synthase
B
NT
CFZ
BDQ
CFZ+BDQ
AMO-1 BTZ-R 91.2 81.4 89.6 16.9 ****
AMO-1 CFZ-R 85.6 86.1 83.3 4.5 ****
RPMI-8226 BTZ-R 94.2 91.1 92.4 28.4 ****
RPMI-8226 CFZ-R 93.0 79.9 92.3 3.2 ****
KMM-1 PIR 96.6 75.7 87.6 22.7 ****
U-266 PIR 95.7 72.4 94.9 6.3 ****
Viability % (+)
100
80
60
40
20
0
C
NT
CFZ
BDQ
CFZ+BDQ
AMO-1 88.0 68.6 86.9 1.7 ****
SK-MM-1 93.9 79.4 93.9 2.2 ****
KMM-1 97.6 91.3 97.7 3.6 ****
RPMI-8226 94.9 60.6 93.8 5.5 ****
NCI-H929 98.3 90.8 96.9 6.9 ****
OPM-2 90.7 65.2 93.8 9.3 ****
KMS-34 87.1 64.4 89.5 17.5 ****
MOLP-8 74.7 71.3 68.9 28.5 ****
JJN-3 95.5 86.3 95.2 36.4 ****
KMS-18 88.5 71.8 87.3 36.1 ****
KMS-11 85.5 75.7 79.0 41.6 ****
U-266 85.9 79.1 82.4 47.0 ****
LP1 81.6 73.5 78.7 54.7 ****
KMS-26 94.6 83.4 91.7 56.5 ****
KMS-28 95.2 67.3 92.3 74.1 ns
K-562 97.1 97.2 88.6 96.5 ns
Viability % (+)
100
90
80
70
60
50
40
30
20
10
0
D
NT
BDQ
CFZ
CFZ+BDQ
GCB-DLBCL
DOHH2 94.4 91.7 89.6 41.9 ****
OCI-LY8 96.3 89.8 84.3 56.8 ****
SU-DHL-6 92.6 80.3 85.2 39.5 ****
SU-DHL-7 95.4 93.5 85.5 56.9 ****
Karpas-422 83.1 80.1 77.7 30.4 ****
ABC-DLBCL
U-2932 88.0 66.4 83.1 51.2 ****
RIVA 80.8 76.0 75.3 3.1 ****
BL
Namalwa 74.3 76.8 66.9 2.8 ****
BL-41 95.8 94.6 85.4 9.6 ****
HS-SULTAN 94.2 88.1 80.1 35.3 ****
Raji 95.1 88.6 90.6 28.6 ****
Daudi 95.2 70.7 87.7 2.8 ****
MCL
Granta-519 92.1 89.1 73.6 26.3 ****
Mino 79.1 53.9 51.8 6.1 ****
AL
ALMC-1 91.5 84.3 81.8 34.4 ****
ALMC-2 96.5 96.5 87.8 13.4 ****
0 20 40 60 80 100
Viability (%)

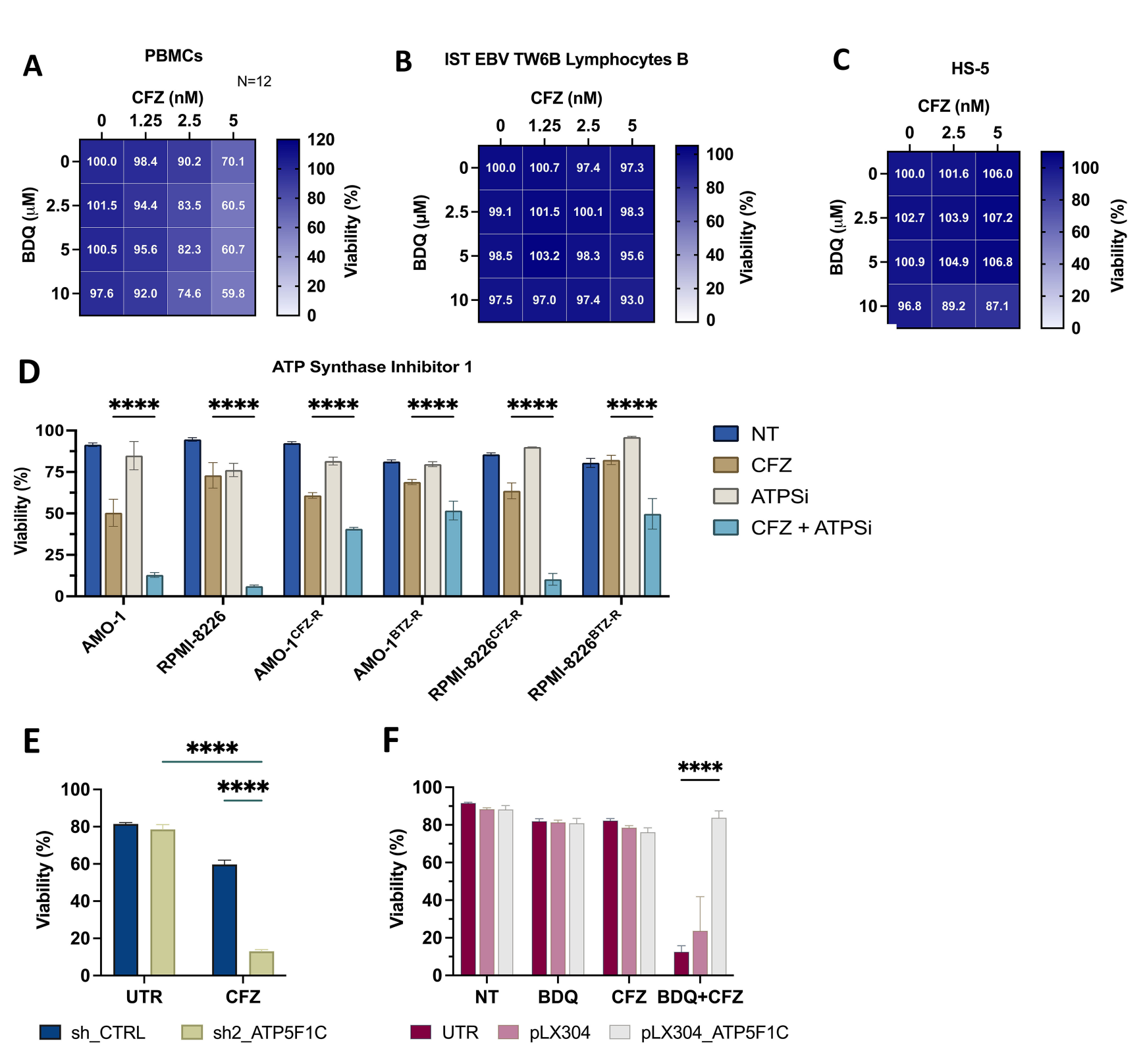
A
PBMCs
N=12
CFZ (nM)
0 1.25 2.5 5
BDQ (μM)
0 100.0 98.4 90.2 70.1
2.5 101.5 94.4 83.5 60.5
5 100.5 95.6 82.3 60.7
10 97.6 92.0 74.6 59.8
120 100 80 60 40 20 0
Viability (%)
B
IST EBV TW6B Lymphocytes B
CFZ (nM)
0 1.25 2.5 5
BDQ (μM)
0 100.0 100.7 97.4 97.3
2.5 99.1 101.5 100.1 98.3
5 98.5 103.2 98.3 95.6
10 97.5 97.0 97.4 93.0
100 80 60 40 20 0
Viability (%)
C
HS-5
CFZ (nM)
0 2.5 5
BDQ (μM)
0 100.0 101.6 106.0
2.5 102.7 103.9 107.2
5 100.9 104.9 106.8
10 96.8 89.2 87.1
100 80 60 40 20 0
Viability (%)
D
ATP Synthase Inhibitor 1
****
Viability (%)
100 75 50 25 0
AMO-1
RPMI-8226
AMO-1CFZ-R
AMO-1BTZ-R
RPMI-8226CFZ-R
RPMI-8226BTZ-R
NT
CFZ
ATPSi
CFZ + ATPSi
E
****
****
Viability (%)
100 80 60 40 20 0
UTR
CFZ
sh_CTRL
sh2_ATP5F1C
F
****
Viability (%)
100 80 60 40 20 0
NT
BDQ
CFZ
BDQ+CFZ
UTR
pLX304
pLX304_ATP5F1C

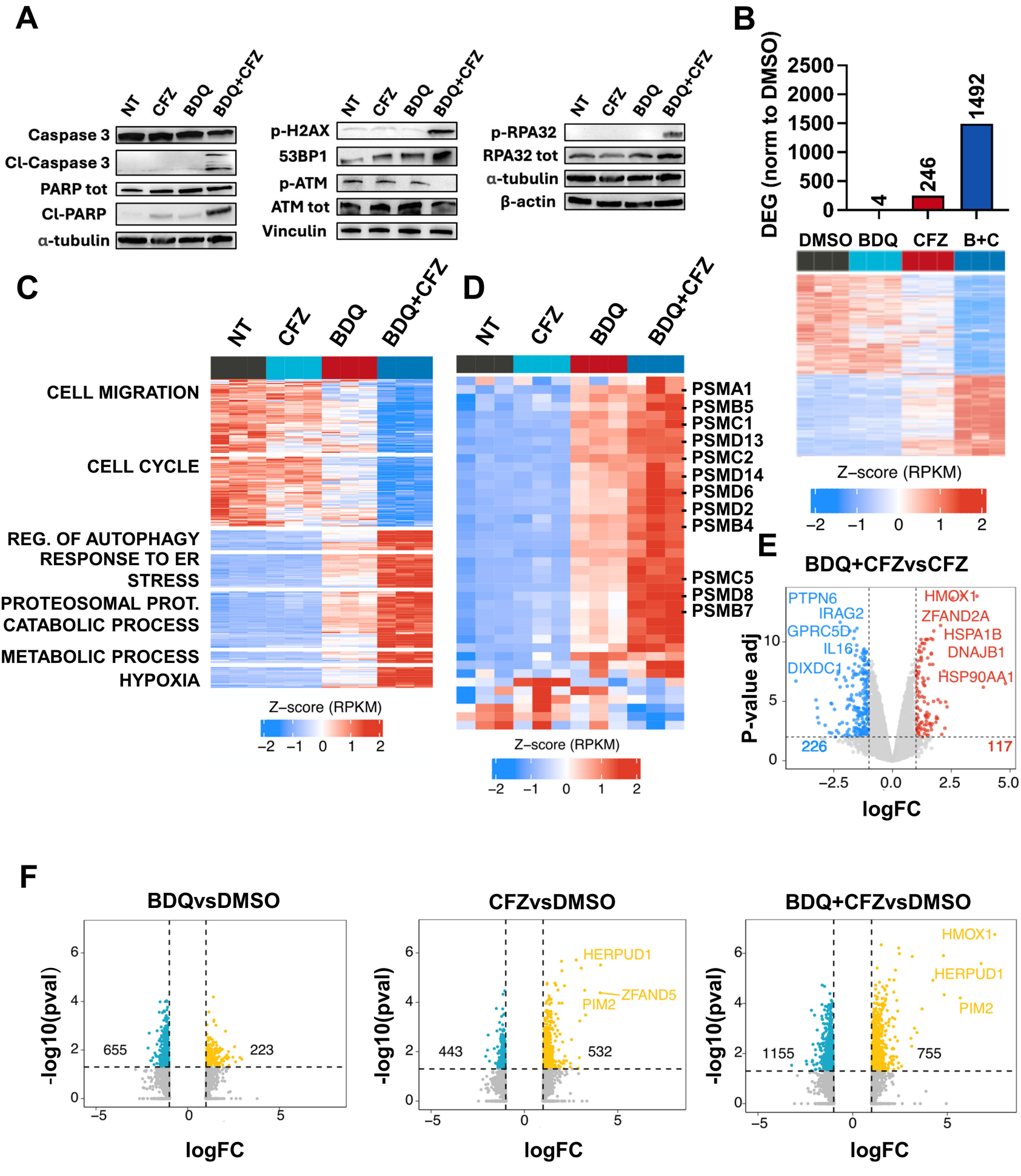
A
NT
CFZ
BDQ
BDQ+CFZ
Caspase 3
Cl-Caspase 3
PARP tot
Cl-PARP
α-tubulin
p-H2AX
53BP1
p-ATM
ATM tot
Vinculin
p-RPA32
RPA32 tot
α-tubulin
β-actin
B
DEG (norm to DMSO)
2500
2000
1500
1000
500
0
4
246
1492
DMSO
BDQ
CFZ
B+C
Z–score (RPKM)
−2 −1 0 1 2
C
CELL MIGRATION
CELL CYCLE
REG. OF AUTOPHAGY
RESPONSE TO ER STRESS
PROTEOSOMAL PROT. CATABOLIC PROCESS
METABOLIC PROCESS
HYPOXIA
Z–score (RPKM)
−2 −1 0 1 2
D
PSMA1
PSMB5
PSMC1
PSMD13
PSMC2
PSMD14
PSMD6
PSMD2
PSMB4
PSMC5
PSMD8
PSMB7
Z–score (RPKM)
−2 −1 0 1 2
E
BDQ+CFZvsCFZ
PTPN6
IRAG2
GPRC5D
IL16
DIXDC1
HMOX1
ZFAND2A
HSPA1B
DNAJB1
HSP90AA1
226
117
P-value adj
10
5
0
−2.5
0.0
2.5
5.0
logFC
F
BDQvsDMSO
655
223
-log10(pval)
6
4
2
0
−5
0
5
logFC
CFZvsDMSO
HERPUD1
ZFAND5
PIM2
443
532
-log10(pval)
logFC
BDQ+CFZvsDMSO
HMOX1
HERPUD1
PIM2
1155
755
-log10(pval)
logFC

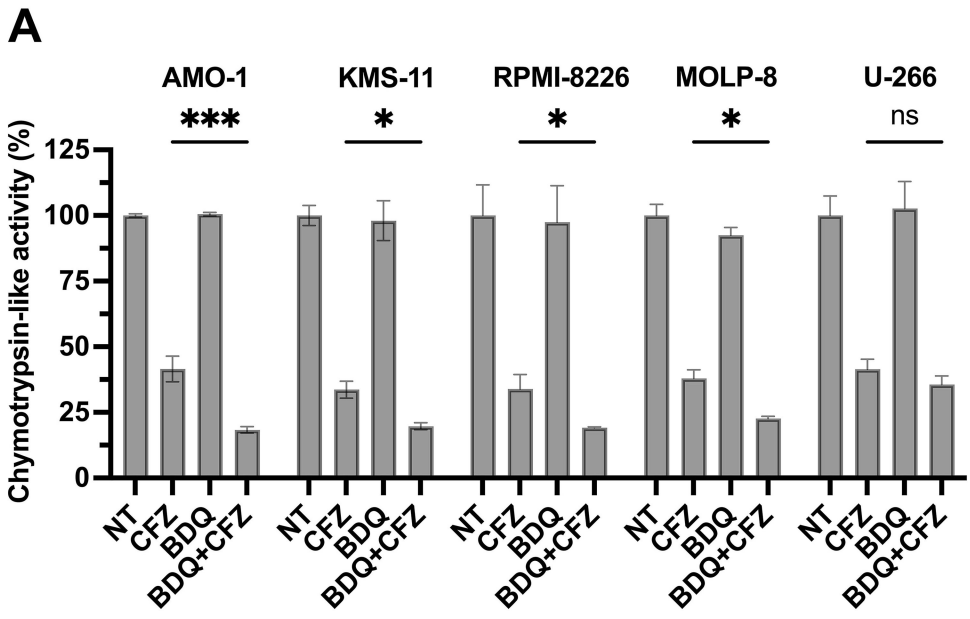

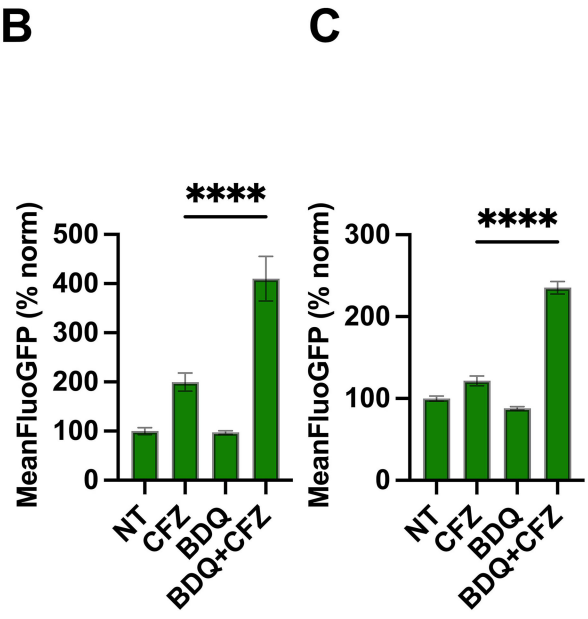

D

AMO-1

		0	1.5nM	2nM	2.5nM	5nM	10nM
CFZ	NT	100.0	83.3	86.9	80.7	57.6	15.3
	+BDQ	91.3	102.0	55.9	28.2	6.4	6.8

		0	1.5nM	2nM	2.5nM	5nM	10nM
BTZ	NT	100.0	92.8	81.9	23.1	1.4	6.1
	+BDQ	91.3	67.8	59.8	21.2	5.2	5.9

		0	1.5nM	2nM	5nM	10nM	20nM
IXA	NT	100.0	88.6	76.8	57.3	8.7	0.5
	+BDQ	91.3	62.2	37.7	30.7	10.2	0.1

		0	1.5nM	2nM	2.5nM	5nM	10nM
MAR	NT	100.0	95.1	84.6	73.4	24.9	10.0
	+BDQ	91.3	74.9	46.2	46.8	13.1	9.9

		0	25nM	50nM	100nM	200nM	400nM
TAK	NT	100.0	87.7	85.7	72.6	56.8	21.1
	+BDQ	96.5	78.9	61.1	18.7	4.7	1.6

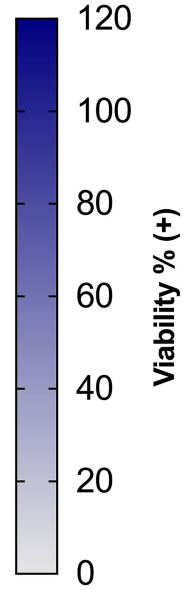

E

AMO-1	BS
BTZ	5.5
IXA	21.1
MAR	14.4
TAK	29.5
CFZ	19.3

F

AMO-1 CFZ-R

		0	50nM	100nM	200nM	400nM	800nM
CFZ	NT	100.0	91.2	71.7	22.7	19.8	3.2
	+BDQ	111.7	15.2	6.7	2.5	6.5	1.6

		0	2.5nM	5nM	10nM	20nM	40nM
BTZ	NT	100.0	111.3	112.5	94.9	36.6	6.4
	+BDQ	93.2	95.5	84.3	40.7	6.3	1.2

		0	12.5nM	25nM	50nM	75nM	100nM
IXA	NT	100.0	90.5	77.1	41.3	22.3	8.6
	+BDQ	111.7	83.2	74.3	33.4	14.8	6.7

		0	1.25nM	2.5nM	5nM	10nM	20nM
MAR	NT	100.0	84.7	67.7	16.5	4.2	1.0
	+BDQ	73.6	72.4	52.6	12.8	4.4	1.4

		0	25nM	50nM	100nM	200nM	400nM
TAK	NT	100.0	103.2	76.2	93.9	25.0	6.2
	+BDQ	111.7	93.4	46.0	11.4	4.9	12.9

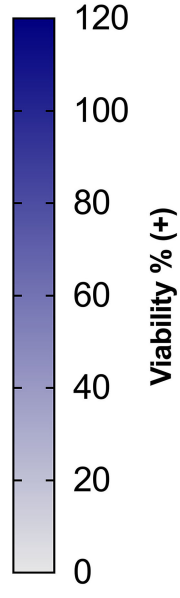

G

AMO-1^{CFZR}	BS
BTZ	21.8
IXA	10.6
MAR	- 3.5
TAK	34.3
CFZ	49.6

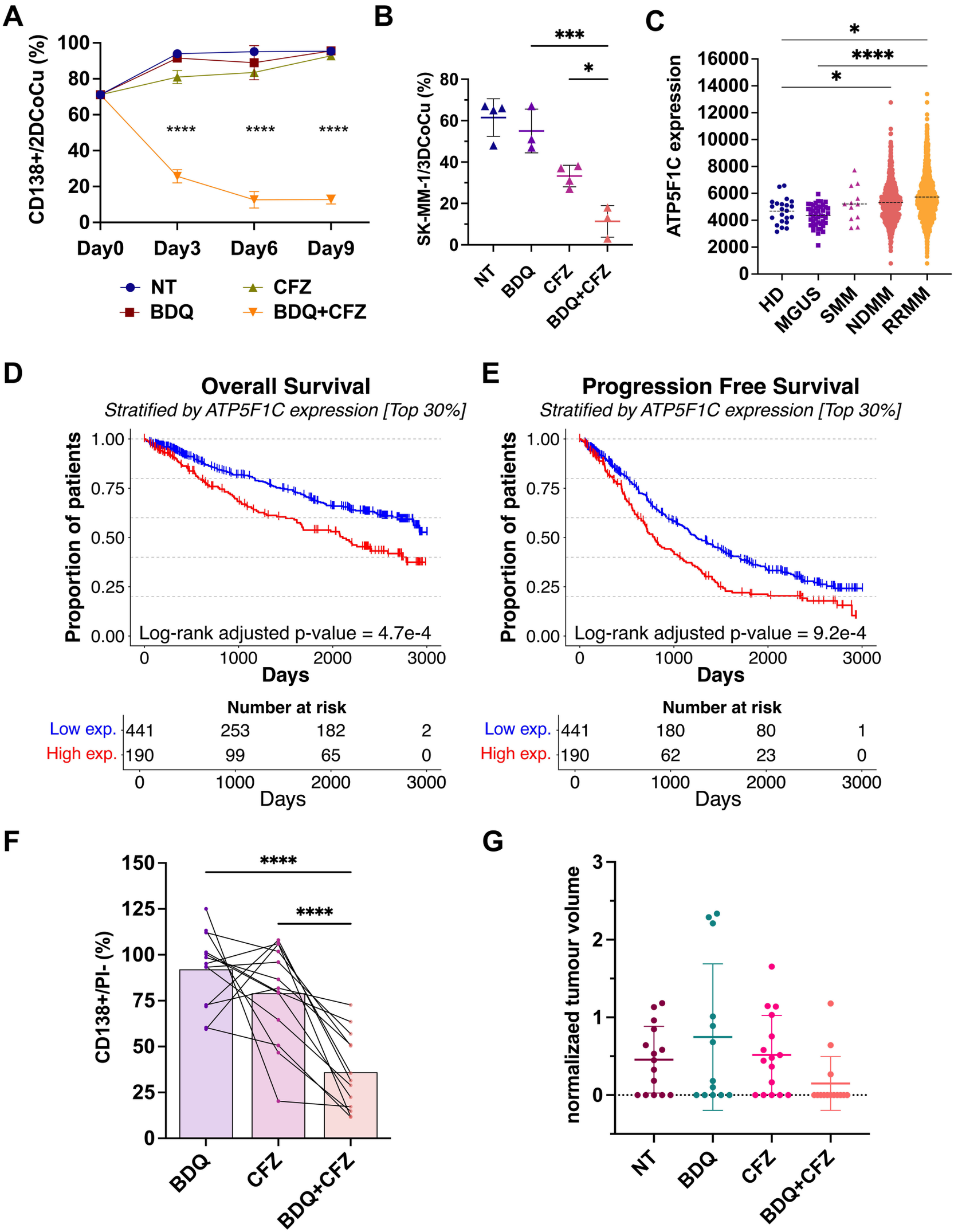
A
CD138+/2DCoCu (%)
Day0
Day3
Day6
Day9
****
NT
BDQ
CFZ
BDQ+CFZ
B
SK-MM-1/3DCoCu (%)
***
*
NT
BDQ
CFZ
BDQ+CFZ
C
ATP5F1C expression
*
****
HD
MGUS
SMM
NDMM
RRMM
D
Overall Survival
Stratified by ATP5F1C expression [Top 30%]
Proportion of patients
Log-rank adjusted p-value = 4.7e-4
Days
Number at risk
Low exp. 441 253 182 2
High exp. 190 99 65 0
E
Progression Free Survival
Stratified by ATP5F1C expression [Top 30%]
Proportion of patients
Log-rank adjusted p-value = 9.2e-4
Days
Number at risk
Low exp. 441 180 80 1
High exp. 190 62 23 0
F
CD138+/PI- (%)
****
****
BDQ
CFZ
BDQ+CFZ
G
normalizaed tumour volume
NT
BDQ
CFZ
BDQ+CFZ

SUPPLEMENTAL MATERIAL

Bedaquiline amplifies proteasome inhibitor efficacy and overcomes resistance in multiple myeloma

Michela Cumerlato[1,2], Monica Maccagno[1,2], María Labrador[1,2], Beatrice Luciano[1,2], Elisabetta Mereu[1,2], Mariangela Porro[1,2], Cecilia Bandini[1,2], Mattia Furlan[3], Domenico Maisano[4], Mattia D'Agostino[1,5], Alessandra Larocca[1,5], Francesca Gay[1,5], Annalaura Tamburrini[2,6], Francesca Anselmi[2,6], Paolo Ettore Porporato[1,2], Salvatore Oliviero[2,6], Benedetto Bruno[1,5], Eugenio Morelli[3,7], Nikhil Munshi[4], Roberto Piva[1,2,5]

[1]Department of Molecular Biotechnology and Health Sciences, University of Turin, Turin, Italy;
[2]Molecular Biotechnology Center (MBC) "Guido Tarone", Turin, Italy;
[3]Candiolo Cancer Institute, FPO-IRCCS, Turin, Italy;
[4]Dana Farber Cancer Institute, Boston, MA, United States;
[5]Città della Salute e della Scienza Hospital, Turin, Italy;
[6]Department of Life Sciences and Systems Biology, University of Turin, Turin, Italy; [7]Department of Oncology, University of Turin, Turin, Italy.

CONTENTS

- Supplementary Figure 6. Representative GSEA enrichment plots in AMO-1 cells
- Supplementary Figure 7. Integrated RNA-seq and proteomics heatmaps highlighting cellular stress–associated gene and protein modulation following BDQ–CFZ treatment
- Supplementary Figure 8. Selective enhancement of chymotrypsin-like proteasome activity by BDQ–CFZ
- Supplementary Figure 9. Synergistic interaction of BDQ with additional proteasome inhibitors
- Supplementary Figure 10. Lack of synergy between BDQ and non-UPS targeting agents
- Supplementary Figure 11. Assessment of stromal and total cell viability in co-culture models following BDQ–CFZ treatment
- Supplementary Figure 12. Independent prognostic impact of ATP5F1C expression in the CoMMpass cohort

Supplementary Tables (provided in a separate Excel file)

- Supplementary Table S1. Top 14 compounds from the secondary drug screen showing synergy with CFZ in five MM cell lines.
- Supplementary Table S2. Cytogenetic and clinical features of MM patients included in ex vivo assays.
- Supplementary Table S3. Concentrations of BDQ and CFZ used for MM cell line treatment and cell viability assay.
- Supplementary Table S4. Concentrations of BDQ and CFZ used for B-cell malignancy cell line treatments and cell viability.
- Supplementary Table S5. Concentrations of BDQ and CFZ used for the treatment of bone marrow-derived mononuclear cells (BMMCs).
- Supplementary Table S6. List of oligonucleotide sequences used in this study.
- Supplementary Table S7. Primary antibodies employed in this study.

SUPPLEMENTARY MATERIALS AND METHODS

Cell Culture Conditions and Reagents

Human multiple myeloma (MM) cell lines, KMM-1, U-266, KMM-1^{PIR}, U-266^{PIR}, KMS-11, NCI-H929, LP-1, AMO-1, OPM-2, KMS-18, KMS-26, KMS-28, KMS-34, RPMI-8226, SK-MM-1, MOLP-8, and JJN-3, along with the murine MM cell line 5TGM1, the chronic myelogenous leukemia cell line K-562, the human stromal cell line HS-5, the Burkitt lymphoma (BL) cell lines (RAJI, HS-Sultan, Daudi, BL-41, and Namalwa), the mantle cell lymphoma (MCL) cell lines (Granta-519 and Mino), and the diffuse large B-cell lymphoma (DLBCL) cell lines including RIVA and U-2932 (ABC-DLBCL), and OCI-LY8, SU-DHL-6, SU-DHL-7, DoHH2, and KARPAS-422 (GCB-DLBCL) were obtained from the DSMZ (Braunschweig, Germany), the ATCC (Manassas, VA, USA), or generated in-house. All cell lines were authenticated by DNA fingerprinting using the GenePrint system (Promega, Madison, WI, USA). Drug-resistant MM lines AMO-1^{CFZ-R}, AMO-1^{BTZ-R}, RPMI-8226^{CFZ-R}, and RPMI-8226^{BTZ-R} were kindly provided by Dr. Lenka Besse (St. Gallen, Switzerland) (1, 2). EBV-immortalized B-lymphocytes (IST-EBV-TW6B) were generously provided by Prof. Valentina Cauda (Politecnico di Torino, Italy). HS-5 (GFP+) cells and RPMI-8226 (tRFP+)-positive cells were derived by transduction with pLKO-GFP and pLemir control vectors, respectively. All cell lines, unless otherwise specified, were cultured in RPMI 1640 (EuroClone, Pero, Italy) supplemented with 10% fetal bovine serum (FBS; Sigma-Aldrich, St. Louis, MO, USA), 2 mM L-glutamine, 100 U/mL penicillin, and 100 µg/mL streptomycin (Gibco). IST-EBV-TW6B cells were maintained in RPMI 1640 with 20% FBS and 1% non-essential amino acids. HEK 293T cells (DSMZ) were cultured in DMEM with 10% FBS and the same supplementation. The AL amyloidosis cell lines ALMC-1 and ALMC-2 were maintained in Iscove's Modified Dulbecco's Medium (Gibco, Thermo Fisher Scientific) supplemented with 10% FBS (Biological Industries), 2 mM L-glutamine, 1% penicillin-streptomycin, 1 ng/mL human interleukin-6 (PeproTech), and 10 ng/ml IGF1. All cultures were maintained at 37°C in a humidified incubator with 5% CO_2. Carfilzomib (CFZ), bortezomib (BTZ), ixazomib (IXA), melphalan (MEL), doxorubicin (DOX), dexamethasone (DEXA), lenalidomide (LENA), venetoclax (VEN), bedaquiline (BDQ), BDQ-fumarate (BDQ-F), and ATP synthase inhibitor 1 (ATPSi) were purchased from Selleckchem (Munich, Germany) or MedChemExpress (Stockholm, Sweden). TAK-243 (TAK) was obtained from TargetMol (Boston, MA, USA).

Synergy Score

Synergistic score of the combinatorial treatment with BDQ or BDQ-F and CFZ was assessed using SynergyFinder+. The score was calculated based on either the Bliss Score (BS) or the ZIP Score.

Virus Production and In Vitro Transduction

High-titer lentiviral stocks were generated in 293T cells by co-transfecting the expression vector (pLKO, pLX304, or pLX301) with packaging vectors (pCMVdR8.74 and VSV-G/pMD2.G), using the Effectene Transfection Reagent (Qiagen, Milan, Italy) according to the manufacturer's protocol. Viral supernatants were collected over 36–60 hours, filtered through a 0.22 µm filter, and concentrated using the Lenti-X Concentrator (ClonTech). Concentrated viruses were resuspended in cold phosphate-buffered saline (PBS) and stored at –80°C. Cells (1 × 10^5/mL) were transduced in the presence of 8 µg/mL polybrene. Fresh medium was added 2 hours post-infection. Stable cell lines were selected using 1 µg/mL puromycin or blasticidin (Sigma-Aldrich). Cell viability was assessed at 48 or 72 hours post-transduction (hpt) using tetramethylrhodamine methyl ester (TMRM; Molecular Probes, Eugene, OR, USA) and flow cytometry.

Gene Silencing and Overexpression of ATP5F1C

Lentiviral vectors encoding short hairpin RNAs (shRNAs) targeting ATP5F1C (shATP5F1C) or a non-targeting control (shCTRL) were generated by subcloning the respective sequences into the pLKO.1-puro vector (Addgene #8453) using AgeI–EcoRI restriction sites. shRNA sequences are listed in Supplementary Table S6. AMO-1 cells were transduced with shATP5F1C or shCTRL lentiviruses, selected with puromycin, and silencing efficiency was confirmed by RT-qPCR and immunoblotting.

For overexpression, the ATP5F1C open reading frame was obtained from the DNASU plasmid repository (pLX304-ATP5F1C, HsCD00441174) and used to produce lentiviruses. AMO-1 cells were transduced with pLX304-ATP5F1C or empty vector (pLX304), followed by blasticidin selection. Overexpression was validated by RT-qPCR and immunoblotting.

Ub-G76V-GFP Proteasome Inhibition Reporter

The pLX301_Ub-G76V-GFP vector was derived from pEGFP-N1-Ub-G76V-GFP (Addgene #11941, gift from Nico Dantuma). For proteasome inhibition assays, MM cell lines AMO-1_UbGFP and AMO-1_UbGFP$^{BTZ\text{-}R}$ were seeded at 1x10^5 cells/mL. AMO-1_UbGFP and AMO-1_UbGFP$^{BTZ\text{-}R}$ cells were treated with 2.5 nM and 12.5 nM CFZ, respectively, 10 µM BDQ, or their combination. Cell viability was assessed by TMRM staining, and GFP-positive cells along with their fluorescence intensity were analyzed by flow cytometry and

fluorescence microscopy using a ZEISS Axio Observer inverted microscope (10× objective) at 10, and 24 hpt.

ATP-Lite Assay

Cell viability/proliferation was measured using the CellTiter-Glo® Luminescent Cell Viability Assay (Promega). Cells were seeded at 1 × 10^5/mL and analyzed at day 0 and at the indicated timepoints. Ten microliters of cells were mixed with an equal volume of CellTiter-Glo® reagent in a white 384-well plate, in technical duplicate. Plates were shaken in the dark for 2 minutes and incubated at room temperature (RT) for 10 minutes. Luminescence was measured using the Synergy™ 2 Multi-Mode Microplate Reader (BioTek Instruments, Winooski, VT, USA).

CCK-8 Assay

Cell viability/proliferation was also assessed using the Cell Counting Kit-8 (CCK-8; Dojindo). Cells were plated at 1 × 10^5/mL and evaluated at day 3 or day 4. 90 µL of cell suspension were mixed with 10 µL of CCK-8 reagent in a 96-well plate, in technical quadruplicate. Plates were incubated at 37°C for 1–4 hours (without CO_2). Absorbance at 450 nm was measured using the Synergy™ 2 reader.

Cell Cycle and Cell Viability Assays by Flow Cytometry

Apoptosis was measured by flow cytometry after staining with tetrametylrodamine methyl ester (TMRM; Molecular Probes, Eugene, Oregon, USA) or Annexin V-FITC Kit (Miltenyi Biotec, Bergisch Gladbach, Germany), according to the manufacturer's instructions. $CD138^+$ cells were identified using anti-human CD138-APC (clone 44F9; Miltenyi). Cell cycle analysis was performed by PI staining. Cells were washed in PBS, incubated with RNase (0.14 mg/mL) and stained with PI (28.57 µg/mL). Data were acquired using BD FACSCelesta™ or BD Accuri™ instruments and analyzed with FACSDiva v8.0 (BD Biosciences).

Proteasome Activity Assay

Chymotrypsin-like, trypsin-like, and caspase-like proteasome activities were measured using the Proteasome-Glo™ Cell-Based Assay (Promega, G1180) according to the manufacturer's protocol. MM cell lines AMO-1, KMS-11, RPMI-8226, MOLP-8, U-266 cell lines were plated at 1×10^5 cells/mL and treated with 2.5 nM CFZ, 5 µM BDQ, or their combination. Proteasome activity was assessed 5 hours post-treatment in technical quadruplicates. For each condition, 50 µL of cell suspension was combined with 50 µL of the appropriate Proteasome-Glo™ reagent (Chymotrypsin-like, Trypsin-like, or Caspase-like) in white 96-well plates. Plates were shaken at 700 rpm for 2 minutes and incubated for

10 minutes at room temperature in the dark. Luminescence was recorded using a Synergy™ 2 Multi-Mode Microplate Reader (BioTek Instruments, Winooski, VT).

Mitochondrial Superoxide Detection

Mitochondrial superoxide was measured using the MitoSOX™ Red Indicator (Thermo Fisher Scientific), according to the manufacturer's protocol, and analyzed by flow cytometry.

Measurement of Oxygen Consumption Rate

Oxygen consumption rate (OCR) was monitored over time using the Resipher™ system (Lucid Scientific, Atlanta, GA, USA). AMO-1 cells were seeded at 20,000 cells/well in 96-well plates and incubated at 37 °C, 5% CO_2. OCR was recorded via the Lucid Lab web app, with data captured every 60 minutes, and monitored for 36 h after treatment with CFZ and BDQ at the indicated concentrations. Measurements are the average of five independent replicates.

immunoBlotting

Cells were lysed in buffer (20 mM Tris-HCl pH 7.4, 150 mM NaCl, 5 mM EDTA, 1% Triton X-100, 1 mM PMSF, 10 mM NaF, 1 mM Na_3VO_4, and protease inhibitors; Roche). Lysates were incubated at 4°C for 30 min, centrifuged at 13,000 × g for 15 min, and protein quantified by Bio-Rad DC assay. Equal amounts of protein were resolved by SDS-PAGE, transferred to nitrocellulose membranes, blocked in 5% milk in PBS-T for 1 h, then incubated overnight with primary antibodies in 5% BSA + NaN_3. Membranes were washed and incubated with secondary antibodies for 1 h, then visualized with Immobilon immunoHRP substrate (Merck). Antibodies used are listed in Supplementary Table S7.

RNA Extraction and Reverse Transcription-quantitative PCR (RT-qPCR)

Total RNA was isolated using the RNeasy Mini Kit (Qiagen). RNA was treated with RQ1 RNase-free DNase (Promega) and reverse-transcribed using the OneScript Plus cDNA Synthesis Kit (ABM, Canada) or SuperScript III (Invitrogen, Carlsbad, CA, USA). RT-qPCR was performed in 384-well plates on a Bio-Rad iCycler using iQ SYBR Green or BlasTaq™ 2X qPCR MasterMix (ABM), following manufacturer instructions. Cycling: 95°C for 10 min, then 40 cycles of 95°C for 15 s and 60°C for 1 min. Primer sequences (designed via PrimerBLAST) are listed in Supplementary Table S6. Specificity was validated by melting curve, standard curve slope, and linearity. GAPDH served as the endogenous control. Expression levels were normalized to control infections (scrambled shRNA, empty vector, or uninfected).

RNA-sequencing

AMO-1 cells were treated with DMSO, CFZ (2.5 nM), BDQ (5 μM), or their combination, and harvested at 6, 12, and 18 hpt. RNA was extracted using the RNeasy Mini Kit and quality assessed via Agilent TapeStation. Libraries were prepared with the TruSeq Stranded mRNA Kit (Illumina) and sequenced on the Illumina NextSeq 1000. Reads were aligned to hg38 using STAR v2.7.1a. Gene counts were obtained with featureCounts v1.6.3 using GENCODE v42 (3). Differential expression was determined by GLM and likelihood ratio tests; genes with |logFC| >1 and FDR <0.01 were considered significant. Gene set enrichment was performed using the SnakeGSEA pipeline with multiGSEA (https://github.com/molinerisLab/SnakeGSEA) (4). Genes were ranked according to the signed statistic derived from the differential expression analysis for each contrast (BDQ vs Ctrl, CFZ vs Ctrl, BDQ-CFZ vs Ctrl). Enrichment was evaluated using gene sets from the Hallmark (MSigDB), KEGG, and Gene Ontology (GO) collections. Default parameters were applied, and statistical significance was assessed based on normalized enrichment scores (NES) and false discovery rate (FDR q-value). Representative enrichment plots were generated for selected pathways of interest. Heatmaps were generated using the ComplexHeatmap R package (5).

Prognostic analysis in the CoMMpass dataset

Gene expression and clinical data were retrieved from the CoMMpass study (IA21 release). Expression levels of ATP5F1A, ATP5F1B, and ATP5F1C (Salmon unstranded TPMs) were obtained together with overall survival (OS) and progression-free survival (PFS) data and corresponding censoring indicators. Patients were stratified according to gene expression levels using the top 30% of each gene expression distribution as the high-expression group. Kaplan–Meier survival curves were generated for OS and PFS, and group differences were assessed using the log-rank test with correction for multiple testing.

To evaluate the independent prognostic value of ATP5F1C, multivariable Cox proportional hazards regression models were fitted including: ATP5F1C expression (top 30% vs remaining patients), age (continuous variable), CGS high-risk classification (binary variable) developed by the International Myeloma Society and the International Myeloma Working Group (6). This classification integrates recurrent cytogenetic alterations and serum biomarkers. CGS status was reconstructed in the CoMMpass dataset using copy number estimates, somatic mutation calls, Seq-FISH data, and baseline clinical measurements. Gene-level copy number values were used as proxies for chromosomal alterations (e.g., CDKN2C for del(1p32), TP53 for del(17p13), and CKS1B for 1q gain). Log_2 ratio thresholds

were applied to define gains and monoallelic or biallelic deletions, consistent with the original publication. Baseline serum biomarker measurements were used for risk classification.

All survival analyses were restricted to 631 patients with complete CGS component data and available ATP5F1 expression levels in CD138-positive bone marrow plasma cells at baseline. The proportional hazards assumption was evaluated using Schoenfeld residuals, and no violations were detected (all p-values > 0.05). Data manipulation, statistical analyses, and visualization were performed in R using the readr, survival, and survminer packages. The R script used for these analyses is available upon request.

Mass Spectrometry (MS) and Proteomic Data Analysis

Cells were lysed by boiling at 95°C for 10 minutes in 100 mM triethylammonium bicarbonate (TEAB) containing 2% sodium deoxycholate (SDC), 40 mM chloroacetamide, and 10 mM tris(2-carboxyethyl)phosphine (TCEP), followed by sonication (Bandelin Sonoplus Mini 20, MS 1.5). Protein concentration was determined using the BCA Protein Assay Kit (Thermo Scientific), and 30 µg of protein per sample was used for MS preparation. The volume was adjusted to 50 µL with 100 mM TEAB containing 2% SDC. Samples were processed using the SP3 protocol, as described by Hughes et al. Briefly, 5 µL of SP3 beads were added to 30 µg of protein, and the final volume was brought to 50 µL with 100 mM TEAB. Ethanol was added to a final concentration of 60% (v/v) to induce protein binding. Samples were mixed and incubated for 5 minutes at room temperature (RT). After magnetic separation, the supernatant was discarded, and the beads were washed twice with 180 µL of 80% ethanol. Proteins were digested on-bead overnight at 37°C using trypsin at a 1:30 enzyme-to-protein ratio, in 100 mM TEAB. Following digestion, samples were acidified to 1% trifluoroacetic acid (TFA) and desalted using in-house packed C18 stage tips (Empore disks (7). Peptides were analyzed by nanoLC-MS/MS using an Aurora Ultimate TS column (25 cm × 75 µm ID, 1.7 µm particles; Ion Opticks). Mobile phase A consisted of water with 0.1% formic acid, and mobile phase B consisted of acetonitrile with 0.1% formic acid. Samples were first loaded onto a trap column (C18 PepMap100, 5 µm, 300 µm × 5 mm; Thermo Scientific) for 4 minutes at 18 µL/min using a loading buffer of water, 2% acetonitrile, and 0.1% TFA. Peptides were then eluted with a linear gradient from 4% to 35% B over 60 minutes. Eluted peptides were ionized by electrospray and analyzed on a Thermo Scientific Orbitrap Ascend in data-independent acquisition (DIA) mode. Survey scans were acquired from 350–1400 m/z at 60,000 resolution (at 200 m/z) with an ion target of 4×10^5. DIA scans were collected at 30,000 resolution with an AGC target of 1000% and maximum injection time set to "Auto." The 400–1000 m/z range was segmented into 30 windows of 20 Da each.

HCD fragmentation was performed at a normalized collision energy of 28%. Data were processed and quantified using Spectronaut 18 in directDIA mode (8). Searches were conducted against the human UniProt database (June 2023 release; 20,605 entries). Enzyme specificity was set to C-terminal cleavage after Arg and Lys, allowing cleavage at proline residues and up to two missed cleavages. Carbamidomethylation of cysteines was defined as a fixed modification; N-terminal acetylation and methionine oxidation were set as variable modifications. False discovery rate (FDR) was controlled at 1% for peptide-spectrum matches (PSMs), peptides, and proteins. Quantification was based on MS2-level data. Precursor and protein posterior error probability (PEP) thresholds were set to 0.01 and 0.05, respectively. Processed data were exported and further analyzed using Perseus v1.6.15.0 (9).

2D Co-culture

HS-5 (GFP^+) and AMO-1 cells were seeded in 24-well plates at 5×10^4/mL and 1×10^5/mL, respectively. Cells were treated with CFZ (2.5 nM), BDQ (5 μM), or the combination at day 0 and 3. Every 3 days, cells were collected and replated. Cell viability was assessed by flow cytometry using propidium iodide exclusion prior to lineage marker analysis.

3D Co-culture

3D scaffolds were prepared following the protocol by Belloni et al. (10) with adaptations for multiple myeloma (MM) cell culture under static conditions. Briefly, scaffold discs were created from Spongostan™ sheets (Ethicon, Inc., Somerville, NJ, USA) using a sterile 4 mm biopsy punch. Each disc was pre-seeded with $2x10^5$ GFP-positive HS-5 stromal cells. After 24 hours, $5x10^5$ tRFP-positive SK-MM-1 cells were added to each scaffold. The scaffolds were then cultured in 1 mL of RPMI-1640 medium in 24-well plates. To minimize the presence of non-adherent cells, the scaffolds were transferred to new wells every 24 hours for three days. Drug treatments were administered 72 hours after seeding the SK-MM-1 cells, using sublethal doses of CFZ, BDQ, or a combination of the two drugs. Six days post-treatment, cells were released from the scaffolds using Liberase™ (25 μg/mL, Merck Millipore, Burlington, MA, USA) and analyzed by flow cytometry to assess the ratio of stromal and tumor cells.

Statistical analyses

Statistical analyses were performed with GraphPad Prism 10 (GraphPad Software Inc.). Statistical significance of differences observed (in both *in vitro* and *in vivo* experiments) was determined by Student t test or one-way ANOVA; differences were considered significant when P value was <.05 (*), <.01 (**), <.001 (***), or <.0001 (****)

SUPPLEMENTAL REFERENCES

1. Besse L, Besse A, Mendez-Lopez M, et al. A metabolic switch in proteasome inhibitor-resistant multiple myeloma ensures higher mitochondrial metabolism, protein folding and sphingomyelin synthesis. Haematologica. 2019; 104(9):e415-e419.
2. Soriano GP, Besse L, Li N, et al. Proteasome inhibitor-adapted myeloma cells are largely independent from proteasome activity and show complex proteomic changes, in particular in redox and energy metabolism. Leukemia. 2016; 30(11):2198-2207.
3. Liao Y, Smyth GK, Shi W. featureCounts: an efficient general purpose program for assigning sequence reads to genomic features. Bioinformatics. 2014; 30(7):923-30.
4. Canzler S, Hackermuller J. multiGSEA: a GSEA-based pathway enrichment analysis for multi-omics data. BMC Bioinformatics. 2020; 21(1):561.
5. Gu Z, Eils R, Schlesner M. Complex heatmaps reveal patterns and correlations in multidimensional genomic data. Bioinformatics. 2016; 32(18):2847-9.
6. Avet-Loiseau H, Davies FE, Samur MK, et al. International Myeloma Society/International Myeloma Working Group Consensus Recommendations on the Definition of High-Risk Multiple Myeloma. J Clin Oncol. 2025; 43(24):2739-2751.
7. Rappsilber J, Mann M, Ishihama Y. Protocol for micro-purification, enrichment, pre-fractionation and storage of peptides for proteomics using StageTips. Nat Protoc. 2007; 2(8):1896-906.
8. Bruderer R, Bernhardt OM, Gandhi T, et al. Extending the limits of quantitative proteome profiling with data-independent acquisition and application to acetaminophen-treated three-dimensional liver microtissues. Mol Cell Proteomics. 2015; 14(5):1400-10.
9. Tyanova S, Temu T, Sinitcyn P, et al. The Perseus computational platform for comprehensive analysis of (prote)omics data. Nat Methods. 2016; 13(9):731-40.
10. Belloni D, Ferrarini M, Ferrero E, et al. Protocol for generation of 3D bone marrow surrogate microenvironments in a rotary cell culture system. STAR Protoc. 2022; 3(3):101601.

SUPPLEMENTAL FIGURES AND LEGENDS

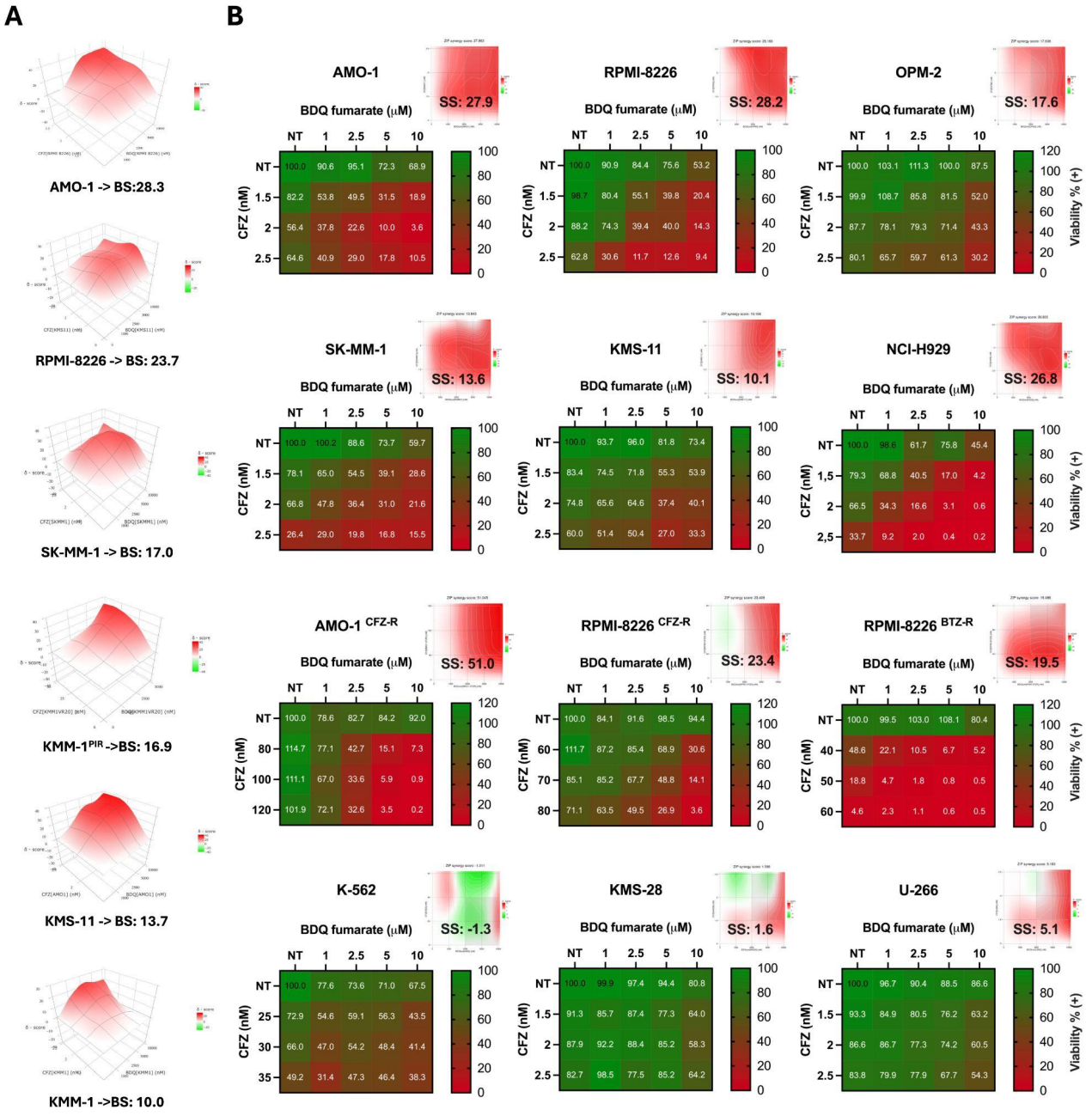

Supplementary Figure 1. Synergistic Effects of Bedaquiline (BDQ) and Its Fumarate Salt (BDQ-F) with Carfilzomib (CFZ) in Multiple Myeloma Cell Lines. (A) 3D dose-response matrices showing the combinatorial effects of BDQ and CFZ in AMO-1, RPMI-8226, KMS-11, SK-MM-1, KMM-1, and KMM-1^{PIR} cell lines. Cell viability was assessed by TMRM staining and analyzed by flow cytometry 72 hours post-treatment. Bliss synergy (BS) scores were calculated using the SynergyFinder+ tool (www.synergyfinder.org). **(B)** Dose-response matrices of BDQ-F and CFZ combinations across a panel of MM cell lines and the K-562 chronic myeloid leukemia cell line. Viability was measured using CellTiter-Glo® Luminescent assay 72 hours post-treatment and normalized to luminescence values at time 0. Synergy scores (SS) were calculated using the Bliss independence model.

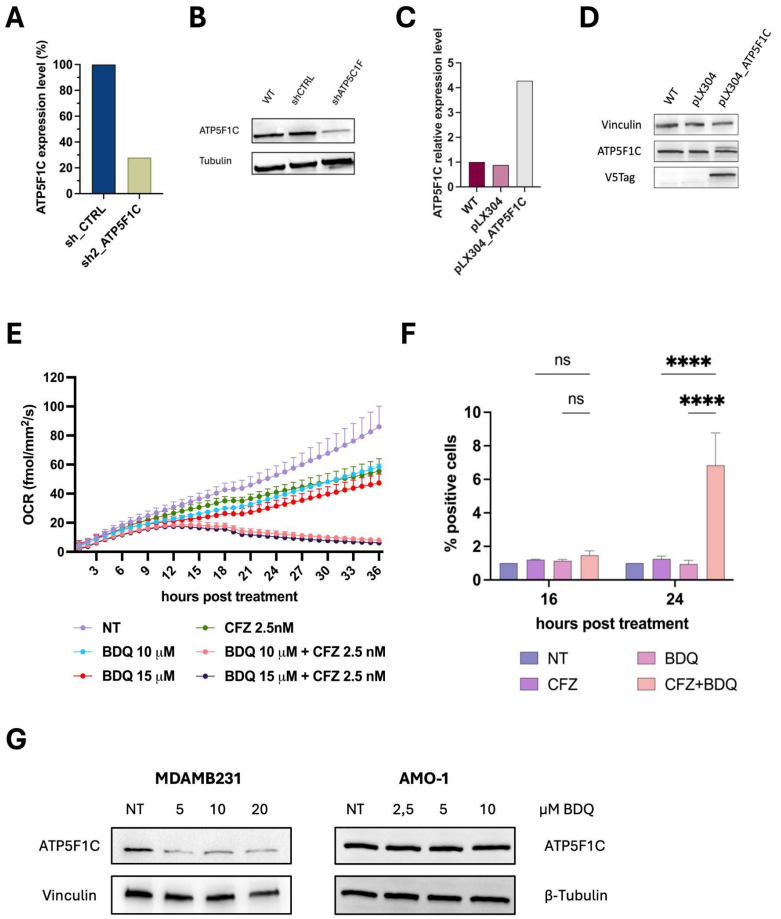

Supplementary Figure 2. ATP5F1C Knockdown and Overexpression Efficiency; BDQ-CFZ Effects on Oxygen Consumption Rate and Mitochondrial ROS Levels. (A) ATP5F1C knockdown efficiency in AMO-1 cells transduced with shRNA targeting ATP5F1C (sh2_ATP5F1C) or scrambled control (shCTRL), quantified by RT-qPCR following puromycin selection. ATP5F1C expression levels were normalized to a housekeeping gene and are shown as relative expression values. Data represent mean ± SD of three independent biological replicates (n = 3). **(B)** Representative immunoblot showing ATP5F1C protein levels in AMO-1 cells expressing shCTRL or sh2_ATP5F1C. α-Tubulin was used as a loading control. **(C)** Relative ATP5F1C expression in AMO-1 cells transduced with empty vector (pLX304) or pLX304_ATP5F1C, assessed by RT-qPCR to confirm overexpression. Expression levels were normalized to a housekeeping gene and are shown as mean ± SD (n = 3). **(D)** Representative immunoblot of ATP5F1C and V5-tag in AMO-1 cells transduced with pLX304 vector or pLX304_ATP5F1C. V5-tag detection confirms ectopic ATP5F1C expression. Vinculin was used as a loading control. **(E)** BDQ–CFZ combination reduced oxygen consumption rate (OCR) compared to single treatments. OCR (fmol/min/mm²) was recorded for 36 hours using the Resipher™ system following treatment with CFZ (2.5 nM) and BDQ (10 or 15 μM) at the indicated concentrations. Data represent mean ± SD of three independent experiments (n = 3). **(F)** Mitochondrial superoxide generation in AMO-1 cells was measured by flow cytometry (MitoSOX staining) at 16 and 24 hours post-treatment with CFZ (2.5 nM), BDQ (5 μM), or the combination. Data are shown as mean ± SD of three independent experiments (n = 3). Statistical significance was determined by one-way ANOVA (****p < 0.0001; ns, not significant). **(G)** Representative immunoblot analysis of ATP5F1C protein levels in MDA-MB-231 and AMO-1 cells following 24-hour treatment with increasing concentrations of BDQ (as indicated). Vinculin (MDA-MB-231) and β-Tubulin (AMO-1) were used as loading controls.

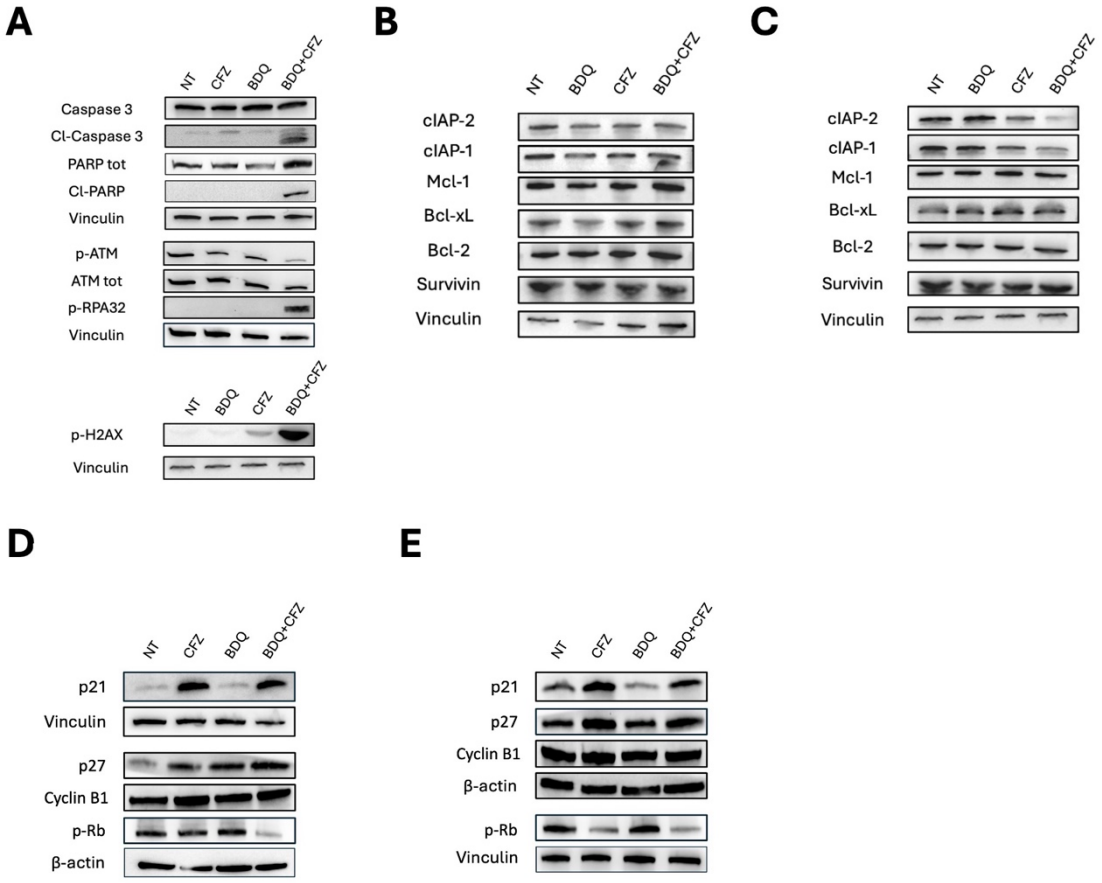

Supplementary Figure 3. Modulation of apoptosis, DNA damage, survival-, and cell-cycle–associated proteins following BDQ and CFZ treatment. (A) Representative immunoblot analysis of apoptosis- and DNA damage–associated proteins in RPMI-8226 cells treated for 16 hours with BDQ (5 μM), CFZ (2.5 nM), BDQ–CFZ, or NT. Cleaved Caspase-3, total and cleaved PARP, phospho-H2AX (γH2AX), phospho-ATM, total ATM, and phospho-RPA32 were assessed as indicated. Vinculin was used as a loading control. **(B–C)** Representative immunoblot analysis of pro-survival and anti-apoptotic proteins in AMO-1 (B) and RPMI-8226 (C) cells treated for 16 hours with BDQ (5 μM), CFZ (2.5 nM), BDQ–CFZ, or NT. Expression levels of cIAP-1, cIAP-2, Mcl-1, Bcl-xL, Bcl-2, and Survivin were evaluated as indicated. Vinculin was used as a loading control. **(D–E)** Representative immunoblot analysis of cell-cycle–associated proteins in RPMI-8226 (D) and AMO-1 (E) cells treated for 16 hours with BDQ (5 μM), CFZ (2.5 nM), BDQ–CFZ, or NT. Expression levels of p21, p27, Cyclin B1, and phospho-Rb (p-Rb) were assessed as indicated. β-actin was used as a loading control.

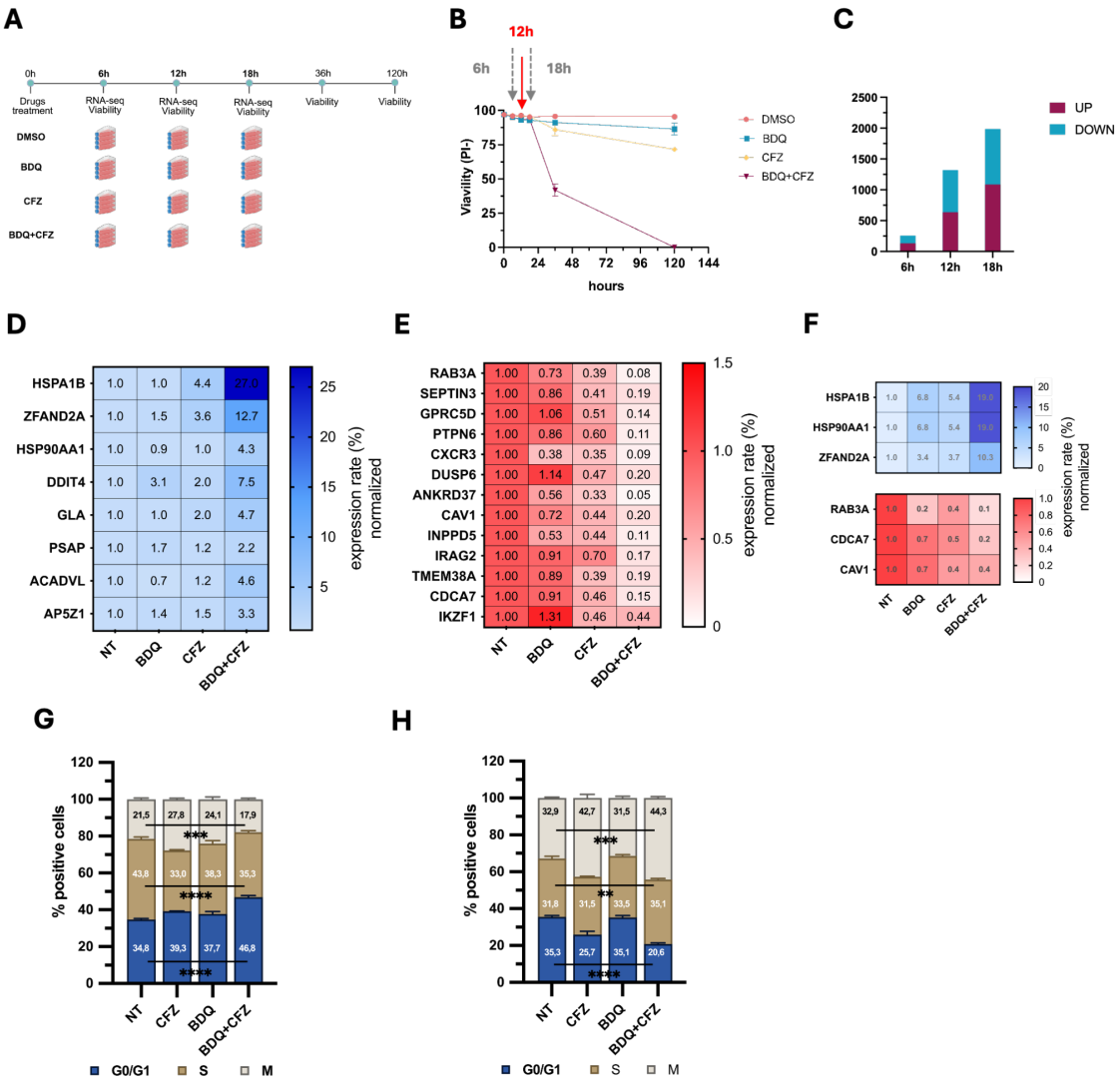

Supplementary Figure 4. RNA-sequencing time course and gene expression validation following BDQ–CFZ treatment. (A) Schematic representation of the RNA-sequencing time course. AMO-1 cells were treated with DMSO, CFZ (2.5 nM), BDQ (5 μM), or the combination (BDQ–CFZ) in biological triplicates. Cells were harvested at 6, 12, and 18 hours post-treatment for RNA-seq analysis, and cell viability was concurrently assessed at 6, 12, 18, 36, and 120 hours post-treatment. **(B)** Time-course analysis of cell viability measured by propidium iodide (PI) staining and flow cytometry. Data represent mean ± SD of three independent experiments (n = 3). **(C)** Bar graph summarizing the number of significantly upregulated (UP) and downregulated (DOWN) genes relative to DMSO at each time point. A total of 133, 637, and 1,087 genes were upregulated, whereas 124, 682, and 899 genes were downregulated at 6, 12, and 18 hours, respectively ($|\log_2 FC| > 1$, FDR <0.01). **(D–E)** Heatmaps showing RT-qPCR validation in AMO-1 cells of selected genes identified as (D) upregulated or (E) downregulated in the RNA-seq dataset following BDQ–CFZ treatment. Expression levels are shown relative to NT and normalized to a housekeeping gene. **(F)** Heatmaps showing RT-qPCR validation in RPMI-8226 cells of three upregulated and three downregulated genes following BDQ–CFZ treatment. Expression values are normalized to NT. **(G-H)** Cell cycle distribution analysis of AMO-1 (G) and RPMI-8226 (H) cells 24 hours after treatment with BDQ (5 μM), CFZ (2.5 nM), or BDQ–CFZ. Cell cycle phases (G0/G1, S, and G2/M) were determined by PI staining and flow cytometry. Data represent mean ± SD of three independent experiments (n = 3). Statistical significance was assessed by one-way ANOVA (****p < 0.0001).

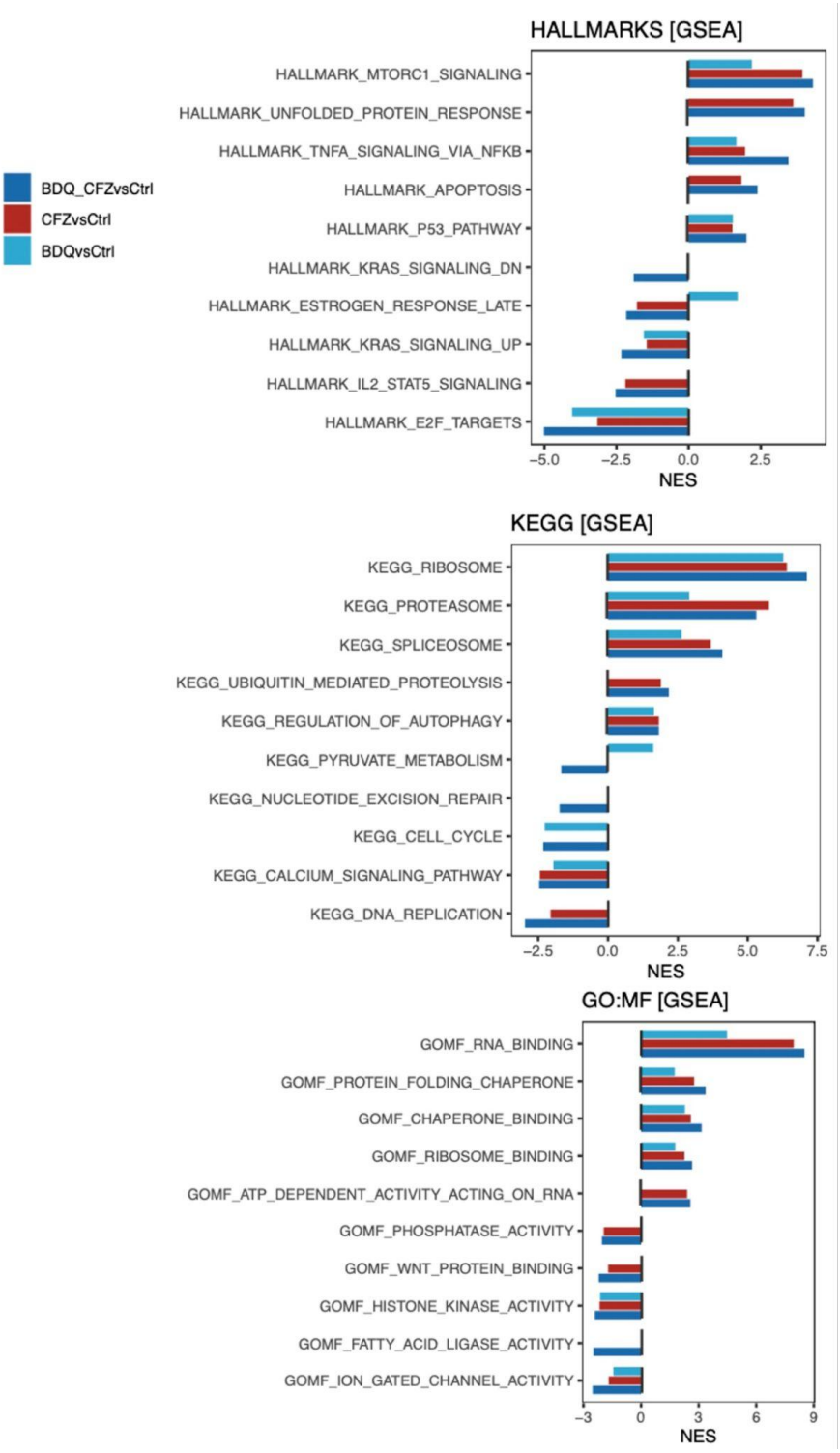

Supplementary Figure 5. GSEA overview in BDQ–CFZ–treated AMO-1 cells. Summary of gene set enrichment analysis (GSEA) from RNA-seq data in AMO-1 cells treated with BDQ, CFZ, or BDQ–CFZ. Barplots display normalized enrichment scores (NES) for selected gene sets from the Hallmark (top), KEGG (middle), and Gene Ontology Molecular Function (GO:MF; bottom) collections across the indicated contrasts. Positive NES values indicate pathway enrichment, whereas negative NES values indicate pathway suppression relative to control.

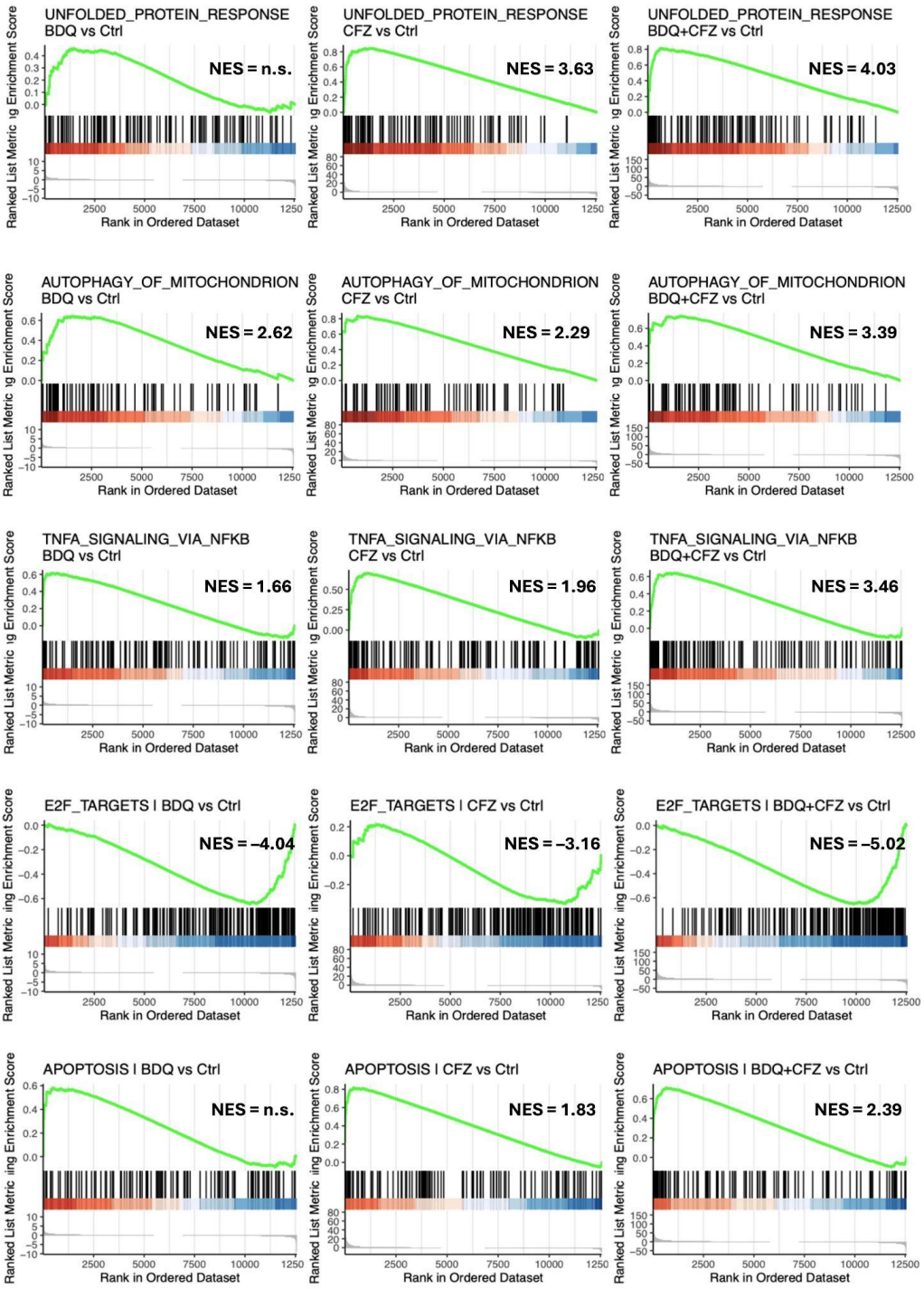

Supplementary Figure 6. Selected GSEA enrichment plots in BDQ–CFZ–treated AMO-1 cells. Representative GSEA enrichment plots from RNA-seq analysis of AMO-1 cells treated with BDQ, CFZ, or BDQ–CFZ. **(A)** Unfolded Protein Response, **(B)** Autophagy of Mitochondrion, **(C)** TNFα Signaling via NF-κB, **(D)** E2F Targets, and **(E)** Apoptosis. For each pathway, enrichment plots are shown for BDQ vs Ctrl, CFZ vs Ctrl, and BDQ–CFZ vs Ctrl, as indicated. Normalized enrichment scores (NES) are displayed within each panel. Positive NES values denote pathway enrichment, whereas negative NES values indicate pathway suppression relative to control.

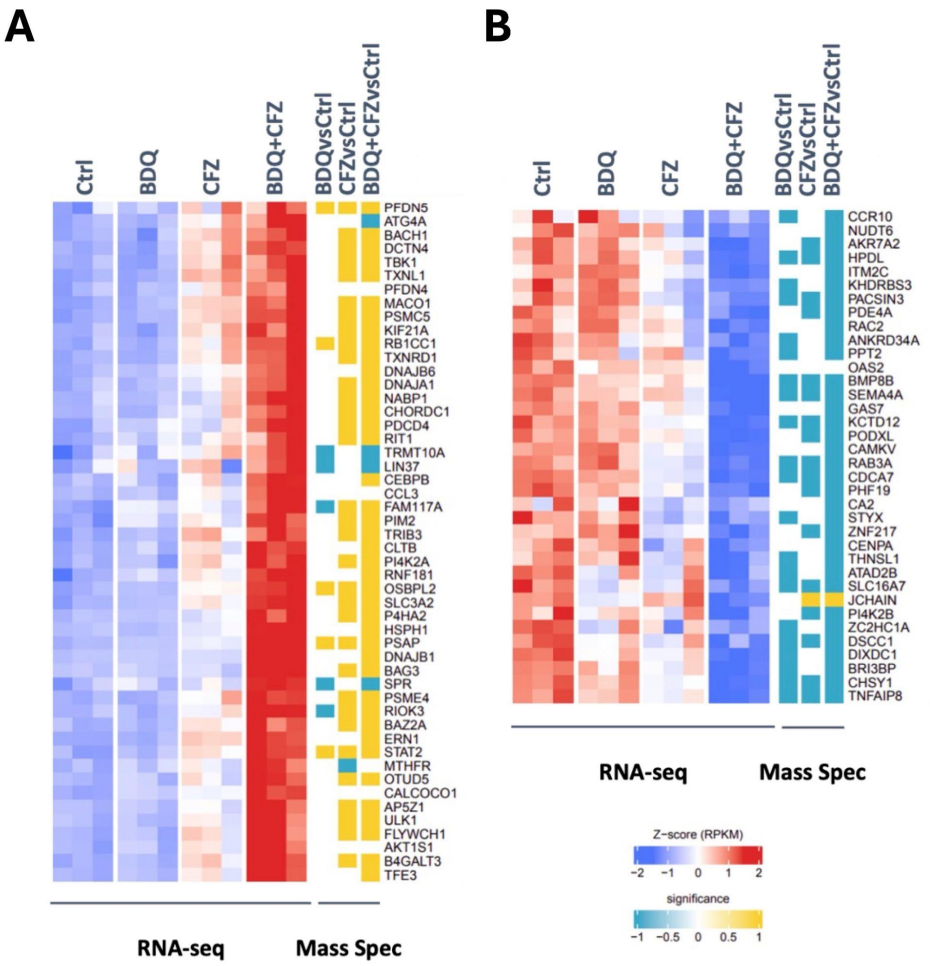

Supplementary Figure 7. Integrated RNA-seq and proteomics heatmaps highlighting cellular stress–associated gene and protein modulation following BDQ–CFZ treatment. (A) Heatmap showing transcripts and corresponding proteins significantly upregulated after BDQ–CFZ treatment, integrating RNA-seq and mass spectrometry datasets. **(B)** Heatmap showing transcripts and proteins significantly downregulated under the same conditions. Gene and protein expression levels are displayed as normalized z-scores (RNA-seq) and normalized protein expression values (mass spectrometry), as indicated by the color scale.

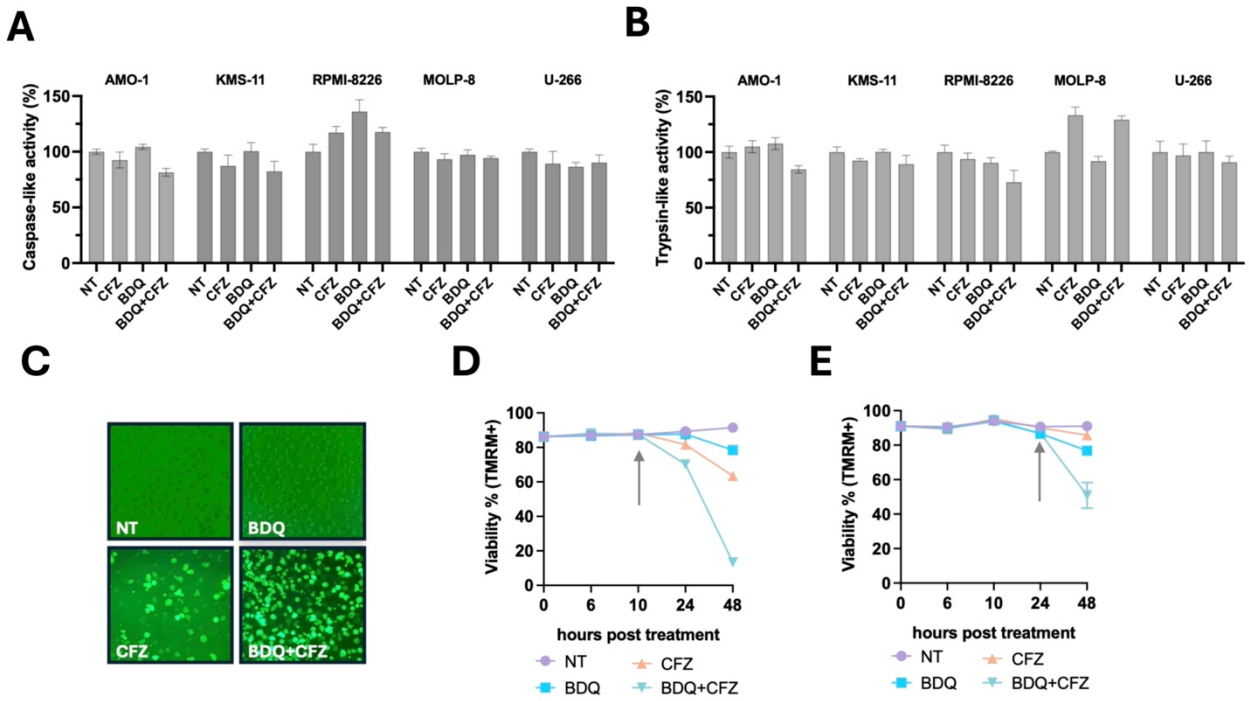

Supplementary Figure 8. BDQ Does Not Interfere with Trypsin-like and Caspase-like Proteasome Activities and Does Not Synergize with Non-proteasome-Targeting Therapies (A-B) Caspase-like **(A)** and trypsin-like **(B)** proteasome activities were measured in AMO-1, KMS-11, RPMI-8226, MOLP-8, and U-266 cell lines following 5-hour treatment with BDQ (5 μM), CFZ (2.5 nM), or their combination. **(C)** Representative fluorescence microscopy images of Ub-G76V-GFP–expressing AMO-1 cells treated with BDQ, CFZ, or the combination, showing marked GFP accumulation in BDQ-CFZ–treated cells. **(D-E)** Longitudinal cell viability analysis of Ub-G76V-GFP-expressing AMO-1 and AMO-1^{BTZ-R} cells treated with BDQ (5 μM), CFZ (2.5 nM for AMO-1 and 12.5 nM for AMO-1^{BTZ-R}), or the combination. Viability was assessed by TMRM staining and flow cytometry at multiple time points. Results represent the mean ± SD of three independent experiments.

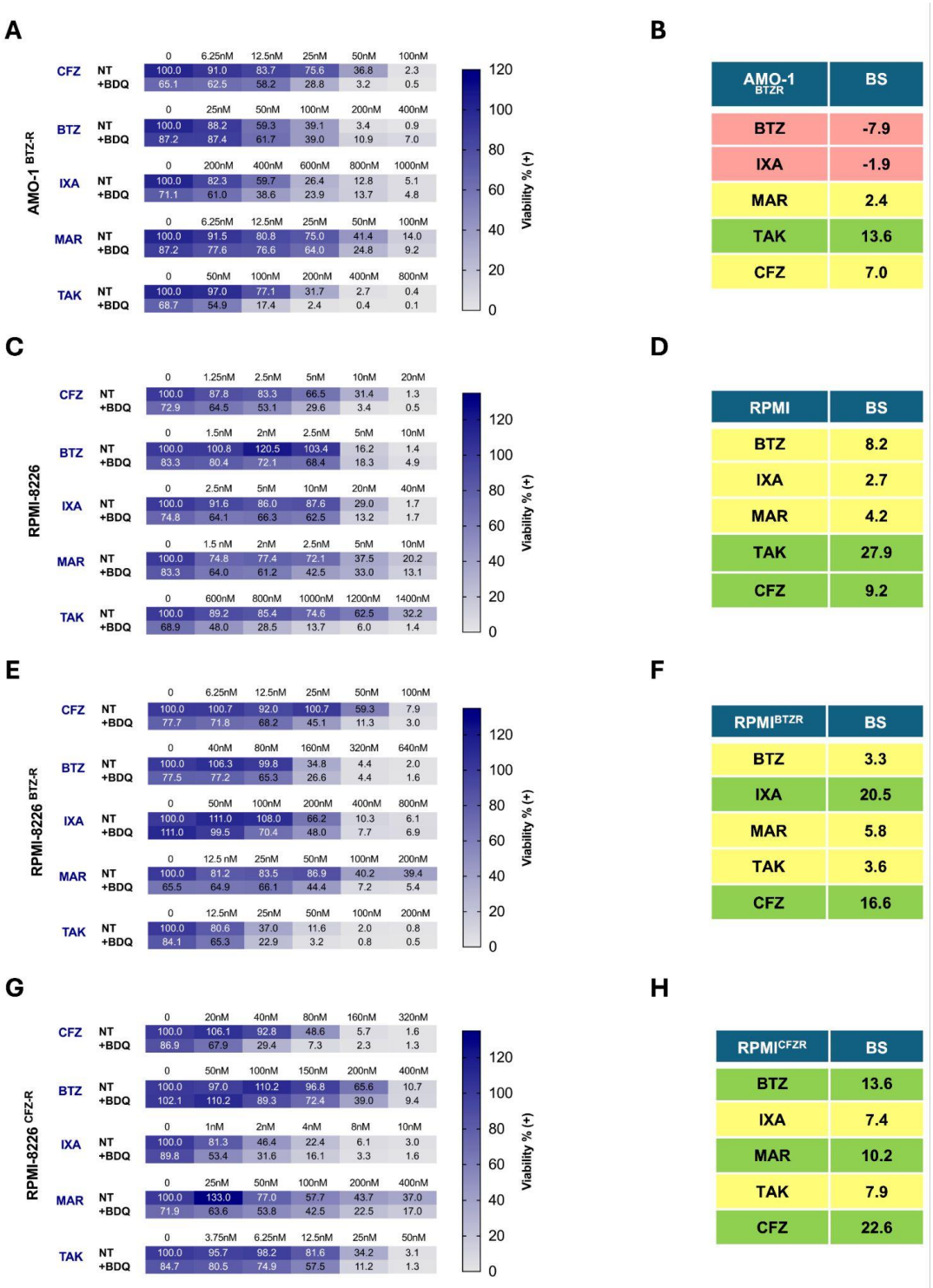

Supplementary Figure 9. BDQ Enhances the Activity of Multiple Proteasome Inhibitors in Both PI-Sensitive and -Resistant MM Cell Lines. Heatmaps of AMO-1^{BTZ-R} **(A)**, RPMI-8226 **(C)**, RPMI-8226^{BTZ-R} **(E)**, RPMI-8226^{CFZ-R} **(G)**, cell lines treated with increasing concentrations of bortezomib (BTZ), ixazomib (IXA), marizomib (MAR), TAK-243 (TAK), or carfilzomib (CFZ), with or without 10 µM BDQ. Cell viability was assessed 72 hours post-treatment by CellTiter-Glo® Luminescent. **(B, D, F, H)** Summary tables reporting the Bliss synergy scores (BS) for each drug combination across the tested cell lines. Green highlights indicate high synergistic interactions (BS > 10), yellow indicates moderate synergistic interactions (1 < BS < 10), while red indicates the absence of synergy (BS < 1).

Supplementary Figure 10. BDQ does not synergize with non-proteasome–targeting therapies. (A) Heatmap of AMO-1 cell viability following co-treatment with BDQ (5 μM) and escalating doses of Venetoclax (VEN), Melphalan (MEL), Dexamethasone (DEXA), Lenalidomide (LENA), or Doxorubicin (DOXO). Cell viability was assessed using CCK-8 assay 72 hours post-treatment.

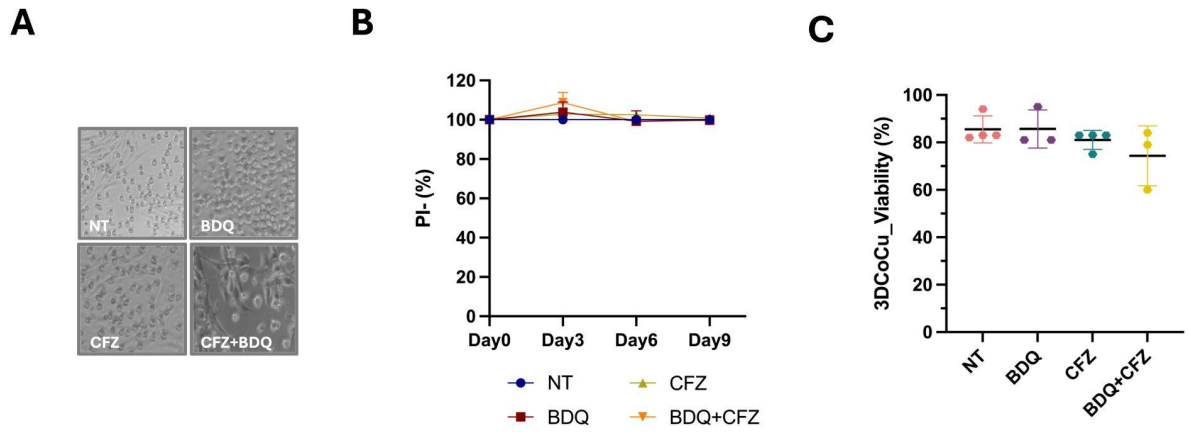

Supplementary Figure 11. Assessment of stromal and total cell viability in co-culture models following BDQ–CFZ treatment. (A) Representative bright-field images of AMO-1 cells cultured on a GFP+ HS-5 stromal monolayer and treated with DMSO (NT), BDQ (5 μM), CFZ (2.5 nM), or the combination (BDQ–CFZ). Images were acquired 3 days post-treatment. **(B)** Viability of HS-5 stromal cells in 2D co-culture following treatment with BDQ, CFZ, or BDQ–CFZ. Cell viability was assessed by propidium iodide (PI) exclusion and flow cytometry. Data represent mean ± SD of independent experiments. **(C)** Total cell viability in the 3D co-culture system (HS-5 and SK-MM1 cells) following treatment with CFZ, BDQ, or BDQ–CFZ. Viability was determined by flow cytometry 6 days post-treatment. Data represent mean ± SD of independent experiments.

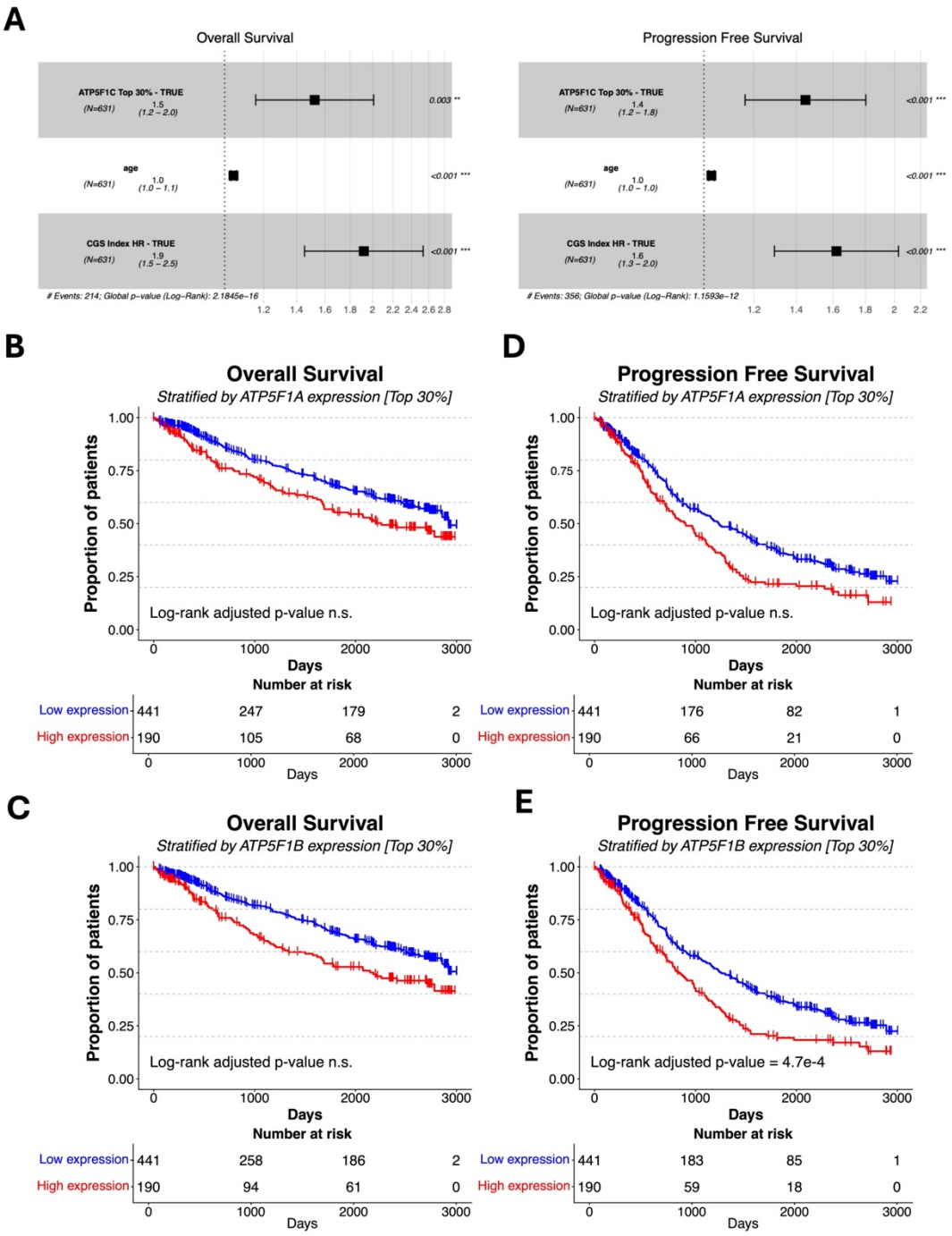

Supplementary Figure 12. Survival analyses and multivariable Cox regression models for ATP synthase subunits. (A) Multivariable Cox proportional hazards regression analysis showing the independent prognostic impact of ATP5F1C expression, age, and CGS high-risk classification on OS and PFS in MM patients from the CoMMpass study (IA21, n = 631). Hazard ratios (HR) with 95% confidence intervals are shown. ATP5F1C expression (top 30% vs remaining patients) and CGS status (high-risk vs standard-risk) were modeled as binary variables. Age was modeled as a continuous variable (per one-year increment). Statistical significance was assessed using the Wald test. **(B-E)** Kaplan–Meier survival curves for OS and PFS according to ATP5F1A and ATP5F1B expression levels in MM patients from IA21 CoMMpass study. Patients were stratified based on the top 30% of gene expression. Statistical significance was assessed using the log-rank test with correction for multiple testing (adjusted significance threshold $p < 0.001$).

Click here to access/download

Supplementary Excel Table

Supplementary Tables.xlsx